IOP Publishing Reports on Progress in Physics
Rep. Prog. Phys. **77** (2014) 056601 (29pp) doi:10.1088/0034-4885/77/5/056601

Review Article

Physics in ordered and disordered colloidal matter composed of poly(*N*-isopropyl acrylamide) microgel particles

Peter J Yunker[1,2], Ke Chen[3], Matthew D Gratale[1], Matthew A Lohr[1], Tim Still[1] and A G Yodh[1]

[1] Department of Physics and Astronomy, University of Pennsylvania, Philadelphia, PA 19104, USA
[2] School of Engineering and Applied Sciences, Harvard University, Cambridge, MA, USA
[3] Beijing National Laboratory for Condensed Matter Physics and Key Laboratory of Soft Matter Physics, Institute of Physics, Chinese Academy of Sciences, Beijing 100190, People's Republic of China

Received 6 August 2013, revised 9 December 2013
Accepted for publication 28 January 2014
Published 6 May 2014

Invited by Paul Chaikin

Abstract

This review collects and describes experiments that employ colloidal suspensions to probe physics in ordered and disordered solids and related complex fluids. The unifying feature of this body of work is its clever usage of poly(*N*-isopropylacrylamide) (PNIPAM) microgel particles. These temperature-sensitive colloidal particles provide experimenters with a 'knob' for *in situ* control of particle size, particle interaction and particle packing fraction that, in turn, influence the structural and dynamical behavior of the complex fluids and solids. A brief summary of PNIPAM particle synthesis and properties is given, followed by a synopsis of current activity in the field. The latter discussion describes a variety of soft matter investigations including those that explore formation and melting of crystals and clusters, and those that probe structure, rearrangement and rheology of disordered (jammed/glassy) and partially ordered matter. The review, therefore, provides a snapshot of a broad range of physics phenomenology which benefits from the unique properties of responsive microgel particles.

Keywords: phase transitions, colloids, colloidal systems

(Some figures may appear in colour only in the online journal)

1. Introduction

In this review article, we describe an emerging class of condensed matter experiment that employs temperature-sensitive suspensions to manipulate and learn about ordered and disordered solids and related colloidal matter. These colloidal suspensions are soft materials composed of responsive particles suspended in water. Of course, the utilization of colloids as model systems to study fundamental problems in statistical physics is not new [1]. Colloids composed of micrometer-sized particles, for example, have taught us a great deal about traditional atomic materials, with particles playing the role of atoms; such colloids are especially useful, because the suspended particles are small enough to experience Brownian motion and large enough to be easily observed and tracked via optical microscopy. In addition, model colloid phenomenology offers a starting point for understanding the physics of a great many soft materials including dispersions, emulsions, pastes, paints, polymers, gels, and liquid crystals, and model colloids provide a bridge to non-equilibrium materials such as granular media and living cells and tissues. Importantly, the colloidal systems permit experimental access to both microscopic and macroscopic information, thus enabling microscopic and macroscopic properties to be directly linked.

Although useful, traditional colloidal media presents significant challenges for the experimenter. Chief among them is the fact that phase behavior in suspension is difficult

to directly control [2]. Phase transitions, for example, are most often induced by increasing or decreasing particle concentration or packing fraction. As such, most experiments on lyotropic systems necessarily employ many samples with many different relative particle volume fractions [3–13], or they employ clever schemes in complex sample cells to alter packing (e.g. osmotic pressure [14, 15] or centrifugation [14, 16, 17]). A few experiments have attempted to directly alter particle interactions, but such experiments are not easy, requiring, for example, gradients in ion concentration, or numerous sets of samples with different particle/solvent properties [18–23].

In light of these complexities, it can be argued that the recent development of temperature-tunable colloidal microgel particles has been a boon for the field. In particular, poly(*N*-isopropylacrylamide) (PNIPAM) hydrogel particles [24–27], and those based on other alkyl substituted polyacrylamides [25, 28–38], are now used as substitutes for traditional suspension constituents. The diameters of PNIPAM spheres vary with small changes in temperature, and this sensitivity provides experimenters with a knob for *in situ* control of the structural and dynamical behavior of colloidal crystals, glasses and liquids [39]. Presently, scientists are utilizing these novel colloids for investigation of fundamental questions about ordered and disordered solid matter, many of which encompass the interests of both hard- and soft-matter physicists stretching from the atomic to granular realms. The purpose of the present review is to provide a snapshot of this activity and thereby stimulate new ideas for use of these novel materials.

Specifically, a brief overview of PNIPAM particle synthesis will be presented, along with information about typical particle properties. The remaining sections discuss experiments that probe crystallization and melting in a variety of geometries, experiments about dynamics and structure and rheology of disordered solids and related complex fluids, experiments that employ PNIPAM particles as depletants for driving phase transitions and cluster formation, experiments that focus on the physics of PNIPAM systems in their own right, and more. Most of this research relies on the temperature sensitivity of the particles, but a few studies also exploit pH sensitivity. Thus the review will travel along a unique trajectory in the soft matter field which teaches a little bit about many current topics, all of which benefit from the unique properties of responsive microgel particles.

2. Properties of PNIPAM particles

PNIPAM hydrogel particles consist of crosslinked PNIPAM polymer chains and water (figure 1). The water has been suggested to be largely immobilized within the particle [24–27] due to strong hydrogen bonds between water and the amide groups of PNIPAM. The interaction between water and PNIPAM is a highly temperature-sensitive balance of hydrophilic and hydrophobic interactions, especially near the lower critical solution temperature (LCST) of approximately 32 °C.

Water is a good solvent for PNIPAM at low temperatures; thus, the polymer network swells (figure 1). When

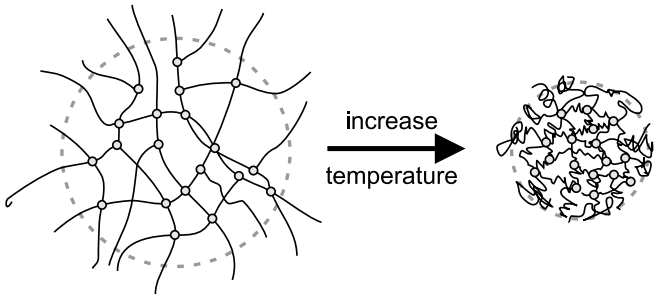

Figure 1. PNIPAM particles depicted in cartoon form. Chains of PNIPAM are crosslinked, and at low temperature the particle diameter is large, because the chains are extended. When temperature is increased, PNIPAM chains coil up, and the particle diameter decreases as a result.

temperature is increased, the polymer becomes increasingly hydrophobic [40], and the polymer chains fold and eventually collapse. Correspondingly, crosslinked hydrogel particles composed of PNIPAM polymer swell to a large diameter at low temperatures, with large numbers of water molecules intercalated into the polymer network structure. At higher temperatures, the polymer chains in the particle become more hydrophobic, and water is (partially) expelled from the particle; thus, the particle diameter decreases with increasing temperature (see figure 1). This thermodynamic effect is brought about by opposing temperature dependencies of the enthalpic and entropic terms of the polymer–water interaction; these effects are discussed in detail in [41].

One result of this peculiar temperature dependence is that the hydrogel particles exhibit a giant thermophoretic effect compared to hard-polymer or glass-like colloid particles [42, 43]. Thermophoretic forces cause suspended particles to move and are brought about by temperature gradients in the sample. Although the exact mechanism of thermophoresis (or Sorét effect) in colloidal suspensions is still debated [44–47], it is clear that the highly temperature-dependent interplay between hydrophobic and hydrophilic polymer–solvent interactions of PNIPAM play an important role enhancing thermophoretic effects.

Arguably the greatest advantage of particles with a temperature-sensitive diameter is that particle volume fraction can be tuned *in situ* [24, 48–50]. In colloidal suspensions, volume fraction is often the primary thermodynamic variable that drives phase behavior. In the case of suspensions composed of temperature-*insensitive* polystyrene, silica and PMMA particles, sample packing fraction is typically tuned by changing the particle number concentration. As a result, many different samples are needed to explore, for example, behavior in the vicinity of a phase transition. With PNIPAM particles, small changes in temperature induce small changes in volume fraction; this capability permits easy study of many volume fractions in the same sample cell, i.e. the same particles can be observed and tracked at different volume fractions.

PNIPAM particles are soft, i.e. they are deformable. One way to characterize particle softness is to examine the interparticle potential, $u(r)$; $u(r)$ is sometimes derived from measurements of the particle radial distribution function $g(r)$ [51]. This method utilizes the fact that in thermal equilibrium

the probability of finding two particles separated by a distance r depends on $u(r)$ in a calculable manner. This approach for determining $u(r)$ works best in dilute samples in which two-body interactions are dominant, e.g. from monolayers of spheres with an areal density of ~10% or less. In this case, $u(r)$ is readily extracted from the measured $g(r)$ by applying liquid structure theory [49]. This approach was employed to obtain the data in figure 2. In this figure, we see that the interparticle potential depends on temperature, and that at temperatures below the LCST, $u(r)$ is short-ranged and purely repulsive; notice also that the tail of $u(r)$ gets stiffer as temperature decreases. For these particles, the effective particle diameter at $1\,k_BT$ is smaller than the hydrodynamic particle diameter measured by dynamic light scattering [24, 49, 52–66] by a factor ranging from a few percent to approximately 10%. Other methods that have been employed to estimate particle softness include the analysis of colloidal particle vibrations [67] and particle centrifugation techniques [68].

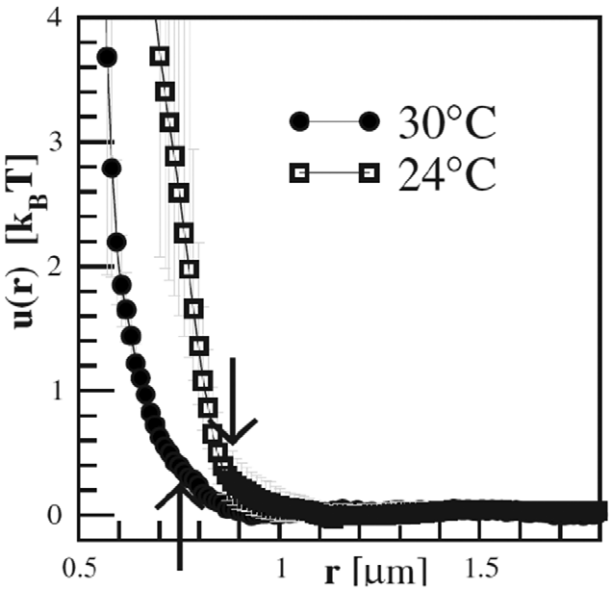

Figure 2. Pair potential $u(r)$ of PNIPAM spheres at 24 °C (squares) and 30 °C (circles). Arrows indicate corresponding hydrodynamic radii measured by dynamic light scattering from dilute suspensions, i.e. the effective radius in the friction factor of particles undergoing Brownian motion. (Figure reproduced with permission from [49]. Copyright 2008 American Physical Society.)

3. Particle synthesis and characterization

This section provides an overview of PNIPAM particle synthesis, and more detailed information about typical particle properties. The particle property characterization, in particular, includes recent results from scattering (i.e. optical, x-ray, neutron), microscopy (i.e. optical and electron) and rheology experiments. These experiments are especially useful for understanding the differences between PNIPAM particles and ideal uniform (hard) spheres, and for understanding the mechanical properties of individual PNIPAM particles and particle suspensions.

3.1. Particle synthesis

PNIPAM microgel particles are usually synthesized by radical emulsion polymerization of *N*-isopropylacrylamide (NIPAM) with crosslinker *N*, *N* -methylenebisacrylamide (BIS) in water at elevated temperature, either in soap-free environments or in the presence of surfactant [25, 69, 70]. (Note, various crosslinking schemes have been employed over the years, e.g., condensation of siloxane-functionalized co-monomers [71], and microwave polymerization schemes [72].) A typical reaction scheme employs surfactant-free radical emulsion polymerization of NIPAM and BIS in water at 60–80 °C using water-soluble initiators such as ammonium peroxodisulfate (APS). APS forms a water-soluble radical that initiates a NIPAM monomer to start a polymer chain. When the PNIPAM chain grows beyond a critical length, phase separation occurs because of the polymer's insolubility in water at the reaction temperature (this process is sometimes referred to as 'precipitation polymerization'). The resulting colloidal particles are stabilized sterically and by charge from the initiator molecules, e.g. negative charge of the sulfate groups of APS. The use of additional surfactant, e.g. sodium dodecyl sulfate, can sometimes improve stability [73].

In practice, the crosslinker often reacts faster than the NIPAM at typical reaction temperatures, producing an inhomogeneous crosslinking density in the microgel particles [73]. When the crosslinking density is higher at the center of the particles, the polymer density in the swollen state is also higher near the particle center. Such heterogeneous polymer distribution within the particle can adversely influence particle mechanical and optical properties [74–77], and a few approaches have been devised to reduce these inhomogeneities. One approach employs a semi-batch procedure. With this scheme, homogeneous, nearly transparent small microgel particles with diameters of order a few hundred nm have been obtained [75, 78]. Very recently, these synthesis schemes have been extended to make nearly transparent, homogeneously crosslinked, spheres in the micrometer-diameter size regime. In particular, a semi-batch method permitting incorporation of co-monomers and the addition of electrolytes was demonstrated to yield uniform PNIPAM spheres with well-controlled diameters ranging from 0.8 to 4 μm [79].

Of course, particle size is influenced by other parameters, including initial monomer concentration, temperature, monomer-to-crosslinker ratio and initiator concentration. For typical reaction conditions, particle diameters are below 1 μm, and the addition of surfactants such as sodium dodecyl sulfate leads to a further decrease of particle diameter compared to surfactant-free polymerization methodologies [73]. To this end, schemes have been explored to increase particle size while maintaining functionality. For example, particles larger than 1 μm can be prepared by adding electrolytes to the solution during polymerization in one-pot syntheses [80]; particle size can be controlled by the electrolyte concentration, albeit at the cost of increased polydispersity. Another approach adds small amounts of co-monomers into the suspensions. Acrylic acid co-monomer leads to highly charged particles,

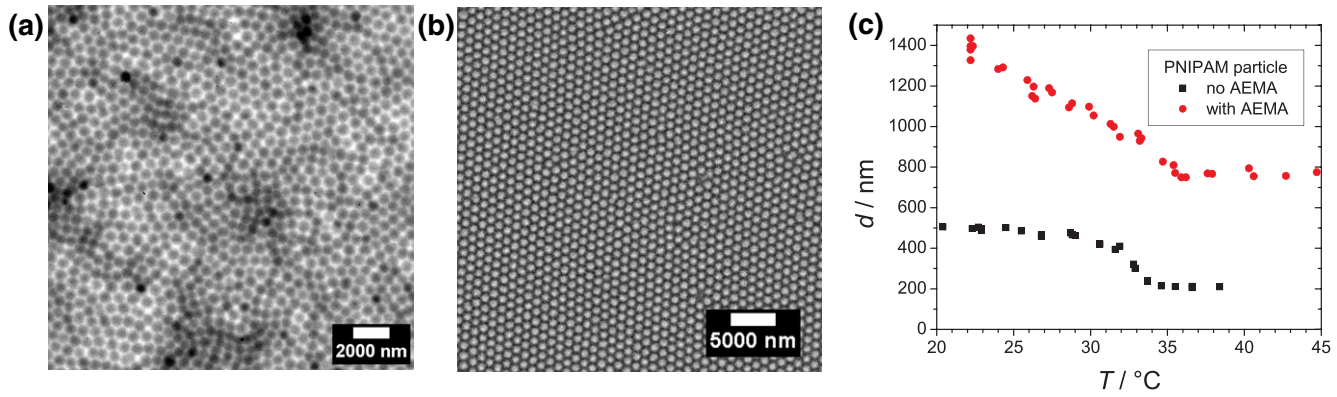

Figure 3. (*a*) Scanning electron micrograph of PNIPAM spheres *in vacuo*. We thank Nicholas Schneider for providing this SEM image. (*b*) Bright-field micrograph of a colloidal crystal monolayer of PNIPAM spheres with $d \approx 1.1\,\mu$m. (*c*) Hydrodynamic diameter, d_h, of different types of PNIPAM particles measured by dynamic light scattering as a function of temperature.

but these particles no longer exhibit a strong temperature-dependence at neutral pH [52, 81]. 2-Aminoethylmethacrylate hydrochloride (AEMA) has also been used as a co-monomer, adding positively charged amine groups to the particle surface [52, 82, 83]. Such particles range in diameter from 1 to 2 μm and are highly temperature-responsive; furthermore, the additional amine groups can be used to functionalize the particles, e.g. with dye molecules.

Much larger particles can be prepared by microfluidic techniques (10–100 μm) [84, 85], or by using calcium alginate as polymerization molds (mm scale) [86]. Syntheses of colloidal composite particles are also described in the literature; core–shell particles with PNIPAM shells, for example, were prepared with silica [87, 88], polystyrene [89] and nanoparticle cores [87, 90–92], and PNIPAM microgel particles were used as starting material to prepare nanostructured PNIPAM–polystyrene particles with adjustable structure [93].

For many (but not all) of the experiments described in this review, typical particle syntheses for the 1–2 μm diameter PNIPAM particles are described in [52] (one-pot synthesis) and in [79] (semi-batch synthesis). These particles can have negative as well as positive surface charge, depending on the choice of initiator and co-monomers.

3.2. Particle characterization

Particle characterization employs a variety of techniques, each with advantages and disadvantages. Per real-space imaging, PNIPAM hydrogel particles can be observed by electron microscopy techniques *in vacuo*, i.e. in the dry state, using standard equipment [94] or cryo-electron microscopy [95–97]. A transmission electron microscopy (TEM) image of particles with $d = 1350$ nm at room temperature is shown in figure 3(*a*); in the dry collapsed state, the particles are about 600 nm in diameter. Environmental scanning electron microscopy has also been used for imaging; in this case, special sample chambers permit control of humidity and, thus, permit electron microscopy of (partially) hydrated microgel particles [98]. Optical microscopy is also utilized to characterize PNIPAM particles in the micrometer range. These particles can be imaged by bright-field microscopy [81, 99] (see figure 3(*b*)) or, if they are dyed, via confocal microscopy.

A qualitatively different, and versatile, method to characterize hydrogel particles is light scattering. Dynamic light scattering measures particle hydrodynamic diameter, d_h, as a function of temperature by quantifying the particle's Brownian motion [52, 100, 101]. The hydrodynamic radius is obtained from a combination of the decay rate of the scattered light intensity temporal autocorrelation function and the Stokes–Einstein equation; d_h corresponds to the best-fit radius of a homogeneous sphere that diffuses against the viscosity of the surrounding solvent and thereby causes the temporal autocorrelation function to decay. The analysis effectively assumes that water molecules inside the microgel spheres are immobilized. In this case, the hydrodynamic properties of the individual particles depend only on sphere diameter. (Note, d_h does not contain information about the polymer density distribution within the microgel particles.)

Two such $d_h(T)$ curves are plotted in figure 3(*c*). The smaller particles were prepared without AEMA and show typical behavior described in the earliest papers: at low temperatures the diameter decreases linearly, but slowly, with increasing temperature. Then, at around the LCST (≈32 °C), the particles collapse, and the diameter decreases rapidly to its high-temperature value. The collapse of colloidal microgels around the LCST is typically not perfectly sharp [25, 78, 91, 102], i.e. it is not as sharp as is often observed for macroscopic PNIPAM gels. Evidently, the crosslinked charged colloids and unconstrained PNIPAM chains differ in their temperature-dependent phase behavior; crosslinking clearly plays a role [25, 91, 103] in affecting the width of the transition. Finally, we note that the role of charge (as introduced by copolymers) in affecting these properties is not fully understood (see the second curve in figure 3(*c*)).

Static light scattering is sometimes used to measure the microgel particle radius of gyration, R_g. The ratio $2R_g/d_h$ was investigated in early work by Senff and Richtering [24, 54] and was found to be 0.6, below that expected for hard spheres (0.778). This deviation was suggested to be a result of decreased crosslinking density in the vicinity of the particle surface. Static light scattering from dilute suspensions yields the particle form factor $P(q)$ as a function of the scattered

wave-vector with magnitude q (as is also the case for small-angle neutron scattering experiments [74]). $P(q)$ depends on the shape of the individual particles as well as the polymer density distribution within the particles. For homogeneous spherical particles, $P(q)$ was calculated exactly by Mie [104], and for some practical applications the simpler Rayleigh–Gans–Debye (RGD) form [105] is a good approximation to the exact result. $P(q)$ for PNIPAM microgel particles, however, is quite often not well fit by the homogeneous forms predicted by Mie or RGD. Instead, models that account for the inhomogeneous polymer density distribution within the microgel particles must be developed and used.

For smaller particles of a few hundred nm in diameter, the particle radius can be extracted from these measurements using the RGD approximation, which is sometimes modified to account for a 'hairy' shell that results from the low crosslinking density in the outer regions of the particles [75–77]. In this way, it is possible to quantify the heterogeneity of polymer density within the particle; in fact, improved homogeneity of semi-batch syntheses was demonstrated using these measurement/analysis schemes [75, 79]. Nevertheless, in order to develop a more detailed picture of the swelling behavior, future studies using temperature-dependent static light scattering [26, 75, 106] could prove useful. In this context, it should be noted that other scattering techniques employing small-angle x-ray [102, 107] and, particularly, neutron scattering [74, 108–111] have been used with success to probe hydrogel material properties at the microscopic scale. Further, atomic force microscopy measurements performed recently by Schmidt *et al* [112] on single PNIPAM particles on a hard substrate agree with the core–shell-like structure found in scattering experiments.

3.3. Rheology

We conclude our characterization discussion with a brief survey of the mechanical properties of hydrogel particles and particle suspensions obtained via rheological techniques. Such experiments were performed on mono- and bi-disperse PNIPAM suspensions in their fluid, crystalline, and jammed states, by application of traditional macrorheology and microfluidic rheology methods.

Traditional (i.e. rheometer-based) macrorheology has been performed on PNIPAM microgel suspensions [24, 58, 113–118, 137] and these samples exhibited many expected changes in shear modulus and viscosity as a function of packing fraction. For example, the shear viscosity, η, was measured as a function of the packing fraction, ϕ, in PNIPAM particle suspensions, and it was found to be similar to that in hard-sphere suspensions for $\phi < 0.5$, indicating that the water within the hydrogel particles is immobilized. For $0.5 \leqslant \phi \leqslant 0.59$, the shape of the $\eta(\phi)$ curves deviated from the hard-sphere models, presumably due to soft-sphere interactions. In the crystalline regime at even higher packing fraction, the samples became viscoelastic, and the shear storage and loss modulus, G and G , were measured; the plateau shear modulus was found to increase as a power law function of ϕ, and G was of the order of a few Pa.

Further work has studied the effects of varying crosslinker density [24, 58], and the behavior of hybrid core–shell particles, which feature polystyrene cores and thermoresponsive hydrogel shells [116, 119, 120]. The core–shell particles were observed to behave essentially like pure hydrogel particles, as long as the particles were only moderately compressed. The packing fraction, ϕ, of these suspensions was varied as a function of temperature and concentration, and it was shown that sample shear viscosity, η, was only a function of ϕ in the fluid regime, i.e. at $\phi \leqslant 0.59$. The behavior for $\phi < 0.5$ was very similar to hard spheres, indicating that the water within the hydrogel particles is immobilized.

The rheological research described above revealed liquid-like and solid-like mechanical behavior in PNIPAM particle suspensions at relatively dilute and dense packings, respectively. Since this early work, interest in thermal (glass-like) and non-thermal (granular-like) jamming transitions and related behavior has undergone rapid progress and has captured the attention of many scientists [19, 21, 122–157]. Concrete predictions, for example, have been made about the scaling of stress versus strain rate in systems near the jamming transition [126, 127, 158–162]. Very recent theoretical/simulation work has suggested that, depending on particle size and interaction strength, colloidal systems under shear at non-zero temperatures can exhibit either thermal (glass-like) or non-thermal (granular-like) transitions or both [129, 155, 154, 163]. In this context, the PNIPAM particle suspensions are proving to be quite interesting; their volume fraction can be tuned around the jamming transition, and their interaction strength and size can be varied, too (e.g. by varying crosslink concentration, etc). Glass-like [117, 119, 137, 154] and critical-point scaling of the stress versus strain rate near the jamming transition [133, 137] has been observed with these systems, and more rheological experiments are in progress. We will discuss this research more in section 6.

Finally, the elastic properties of *individual* PNIPAM particles have been studied. Capillary micromechanics techniques have found that the shear modulus increases with temperature, and the compression modulus dips near the LCST. This leads to a dip in the Poisson ratio, i.e. the ratio of transverse to axial strain, to a low value of ~0.15 near the LCST [164]. In a different vein, clever centrifugation techniques have been developed and employed to measure individual particle elastic moduli [68], and these studies have determined the moduli of a particular set of 1.2 μm-diameter PNIPAM particles to be ~25 kPa. An interesting approach recently applied by Scheffold *et al* [165] and Romeo and Ciamarra [166] is to model the elastic properties of PNIPAM suspensions starting from the individual particle properties, assuming brush-like interactions between touching particles.

4. Behavior near the deswelling temperature

PNIPAM particles exhibit interesting properties near their deswelling temperature of approximately 305 K. Hashmi and Dufresne found that particles are significantly stiffer at high temperatures when particles are fully collapsed, than at lower

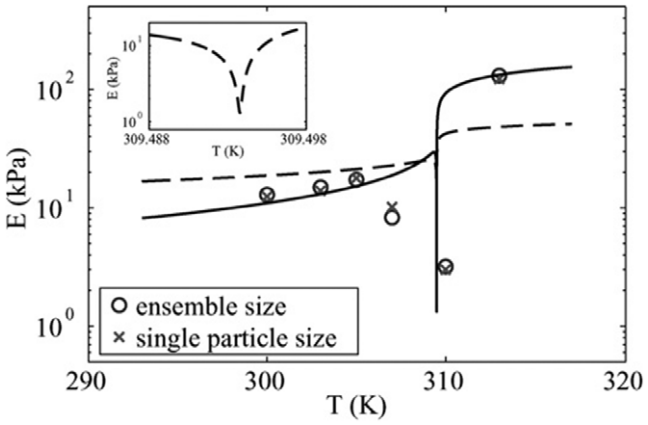

Figure 4. Young's modulus of single PNIPAM microgels as a function of temperature. Open circles denote modulus extracted with ensemble particle measurement of size, and crosses denote modulus extracted with single particle measurement of size. Solid and dashed lines represent fits from theory. Inset shows 0.01 K region around transition temperature of dashed line fit. Reprinted with permission from [121]. Copyright 2009 Royal Society of Chemistry.

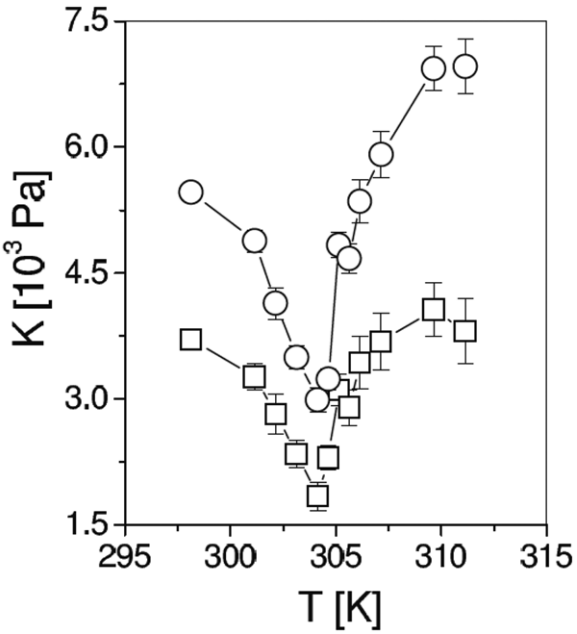

Figure 5. Bulk modulus of PNIPAM–PEG microgels as a function of temperature. Open squares represent particles compressed by 15%. Open circles represent particles compressed by 30%. Solid lines are to guide the eye. (Figure is reproduced with permission from [167]. Copyright 2011 American Physical Society.)

temperatures when the particles are swollen. The particles were also dramatically softer near their deswelling transition [121]. In these experiments, atomic force microscopy was employed to measure the Young's modulus E of individual PNIPAM microgel particles of diameter ≈500 nm (figure 4). When fully swelled, $E \approx 13$ kPa. E was found to increase monotonically with temperature until the deswelling temperature. Near the deswelling temperature, the Young's modulus dramatically decreased to $E \approx 3$ kPa. Then, above the deswelling transition, when the particles are completely collapsed, the Young's modulus was nearly ten times larger than below the transition, i.e. $E \approx 123$ kPa. In further support of these findings, Fernandez-Nieves *et al* determined the bulk modulus, K, of individual PNIPAM microgels (figure 5) by measuring the particle size as a function of external osmotic pressure; they observed that K also drops from approximately 5 to 2.5 kPa near the deswelling transition [167].

Similarly, the elastic moduli of individual macroscopic PNIPAM particles were measured by capillary micromechanics [164]. Voudouris *et al* found bulk and shear moduli in the kPa range and observed a dip in K and Poisson's ratio at the deswelling temperature. They explained these findings qualitatively by Flory–Rehner theory.

5. Phase behavior of colloidal crystals

Colloidal crystals have proven to be useful model systems for studying some of the most basic problems in statistical mechanics, such as the hard-sphere fluid–crystal transition. Crystals composed of PNIPAM particles offer the ability to first load a suspension into a sample chamber at low volume fraction, and then use temperature tuning to create uniform and non-uniform crystals in a variety of geometries. Further, video microscopy is readily utilized to track 'thermal' colloidal 'atoms' in the sample. In this section we give examples of how such crystals are made, and then we discuss new physics that has been learned from these novel crystalline particle suspensions.

5.1. PNIPAM crystal preparation

Many techniques have been employed to prepare PNIPAM colloidal crystals. Joshi *et al* produced crystals by slowly cooling the sample and allowing it to equilibrate over 8–10 hours [325]. Nguyen *et al* studied the growth of PNIPAM crystals created in a temperature gradient [168] and have produced some of the largest crystals therein. Specifically, they applied a temperature gradient of 2 °C cm^{-1} to a sample cell containing a PNIPAM suspension. When the average temperature of the suspension is slowly lowered, nuclei begin to appear near walls of the cell at its cold end (figure 6). Crystalline regions continue to grow from these nuclei as the sample temperature is further lowered, and sometimes large millimeter-sized crystalline domains are formed. These crystals generally exhibit a random hexagonal closed-packed (rhcp) structure, with hexagonal planes parallel to the cell wall. Interestingly, Nguyen *et al* were able to determine the chemical potential difference between crystalline and fluid phases, as well as the orientational anisotropy of the interfacial free energy.

A fast way to prepare PNIPAM crystals is by shearing a concentrated suspension along a flat surface (e.g. [83]). In one incarnation of the scheme, a PNIPAM suspension is injected through a small channel (approximately 50 μm thick) formed by placing two spacers (e.g. strips of stretched parafilm) between a microscope slide and a coverslip; such loading is achieved either by external pressure or by capillary forces. Three-dimensional (3D) crystals with their 1 1 1

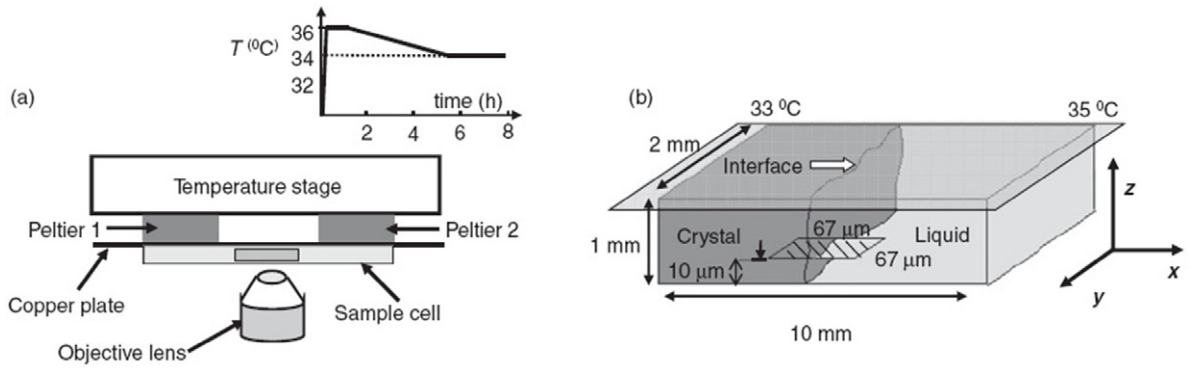

Figure 6. Preparation of PNIPAM colloidal crystals using temperature gradient. (*a*) Experiment schematics: two Peltier plates are used to maintain a temperature gradient in the sample cell. (*b*) Growth of PNIPAM crystal: crystals grow from the cold end of the cell, and the interface moves against the temperature gradient direction as the average sample temperature is lowered. The inset shows the temperature protocol for the growth of a single PNIPAM crystal. (Figure is reproduced with permission from [168]. Copyright 2011 American Physical Society.)

surface parallel to the flow direction are formed in this process. Note, very recently, small-angle x-ray scattering has been used to investigate the crystal structures of hydrogel particles at different concentrations [107]. In these experiments, crystals were prepared in quartz capillaries. In particular, this study showed the formation of probably metastable body-centered-cubic crystal phases at certain packing fractions; these findings are incompatible with hard-sphere-like behavior and are another example of novel soft-matter physics probed by PNIPAM microgel systems.

It is even easier to prepare two-dimensional (2D) crystals. A tiny drop of PNIPAM suspension ($\sim$0.5 μl) placed between a glass slide and a free coverslip will spread under capillary forces and gravity, thus shearing the suspension to form 2D hexagonally packed crystals. Because of the rather short time scale over which the sample is sheared, samples prepared by this method often contain many defects, and crystalline domain sizes are not very large.

Generally, defects can be reduced and domain size increased by mechanical vibration or thermal annealing. Crystal domains greater than a few hundred particle diameters are easily achievable, and the patient experimenter can make much larger crystalline domains. Sample polydispersity also needs to be small for PNIPAM particle to form crystals [326, 327], i.e. a polydispersity less than 5% usually produces crystalline samples.

Very recently, binary crystals were formed with two sizes of PNIPAM particles [321]. The particles were heated and then cooled very slowly, allowing the two sizes of particles to crystalize, as indicated by a sharp Bragg diffraction peak.

5.2. Pre-melting and superheating

Alsayed *et al* studied 'first' melting phenomena (or so-called pre-melting) within 3D PNIPAM crystals [83]. These samples were composed of PNIPAM particles with approximately 375 nm radius; they were prepared using the loading, shearing and annealing methods described above. The crystal melts when the temperature is gradually increased, and the trajectories of individual particles deep in the sample were recorded using bright-field video microscopy. The use of bright-field microscopy is possible because of the close refractive indices of PNIPAM particles and water, but one must be careful when interpreting the images. Interestingly, just before the sample temperature (i.e. sample volume fraction) reached the melting point for the bulk crystal, it was discovered that some regions within the PNIPAM crystal had melted, e.g. corresponding to so-called 'first' melt or pre-melt regions shown in figure 7. These regions always formed close to lattice defects, such as grain boundaries and dislocations. These 'first' melted regions reduce interfacial free energy within the solid and spread further into the bulk as the temperature increases. The study thus revealed an important melting mechanism that might be present in any thermodynamic crystal, but that has been difficult to access in studies of atomic and molecular crystalline materials.

More recent experiments along these lines have discovered that when poly-crystal PNIPAM samples are sheared, grain boundary mobility is highly anisotropic [169]. Specifically, grain boundaries that run perpendicular to the direction of shearing experience significantly more roughening than grain boundaries that are oriented parallel to the direction of shear.

In a different vein, scientists have inquired about the possibility of crystal superheating [171–174]. Indeed, while liquid supercooling is a common phenomenon that often occurs because of crystal nucleation barriers, effects such as surface and grain-boundary pre-melting reduce barriers for melting, so that crystal superheating is rare. If a crystal with nearly perfect lattice structure is heated above its bulk melting temperature and does not melt, then it is said to be superheated. PNIPAM suspensions offer the opportunity to explore these phenomena. Wang *et al* recently reported and studied such superheated colloidal crystals [170].

In their experiments, PNIPAM crystals with large domains were prepared by shearing PNIPAM suspensions in a narrow channel. Then, homogeneous heating of the sample was realized by shining a focused beam of light onto a small region within a much larger bulk crystal; this approach avoided surface melting often caused by directional heating. The

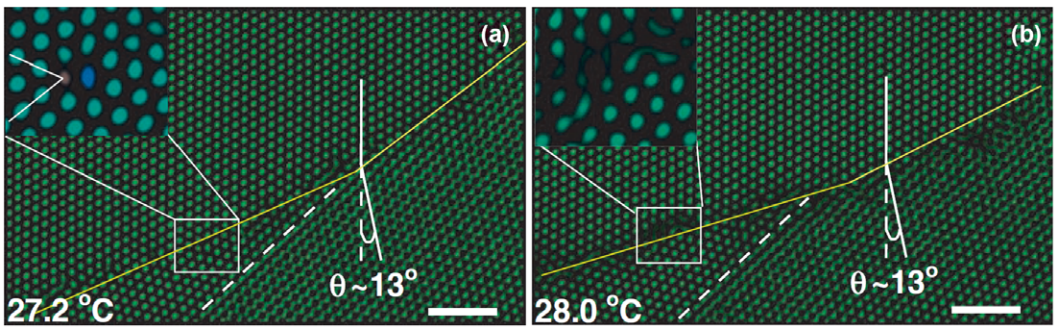

Figure 7. Pre-melting or first melting of the PNIPAM crystal at a grain boundary. The figure shows bright-field images at different temperatures (i.e. particle volume fractions) of two crystallites separated by a grain boundary (crystallites tilted at an angle $\theta = 13^{\circ}$ with respect to one another). (*a*) Sample at 27.2 °C. The solid and dashed lines show the grain boundary and a partial dislocation, respectively. The grain boundary cuts the two crystals along two different planes (the yellow line has two slopes). It is composed of an array of dislocations; the two extra planes are indicated by lines in the inset. (*b*) Sample at 28.0 °C. The particles in the vicinity of the grain boundary start to melt first; nearby particles undergo liquid-like diffusion (inset). The partial dislocation, denoted by the dashed line, is not affected. Scale bars, 5 μm. (Figure is reproduced with permission from [52]. Copyright 2011 Wiley.)

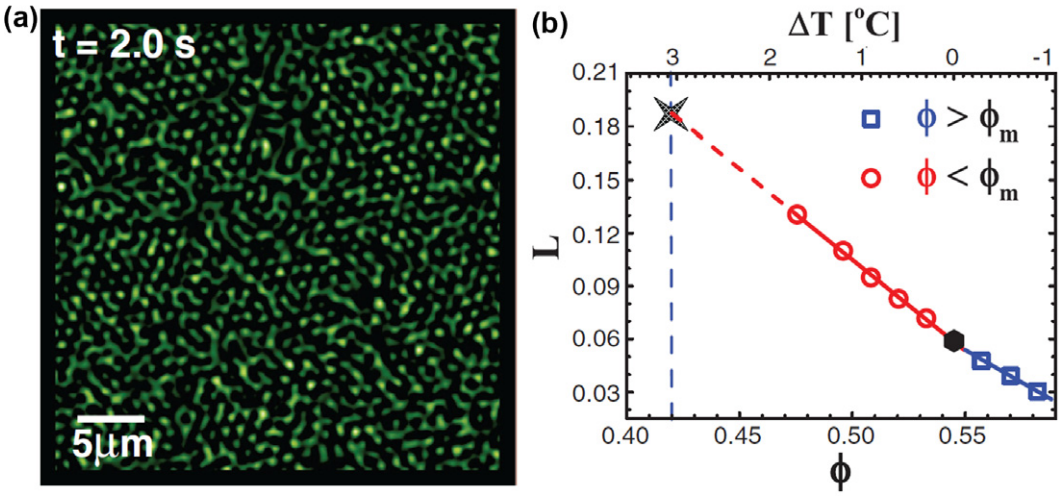

Figure 8. Homogeneous superheating of a bulk PNIPAM crystal. (*a*) A PNIPAM crystal melts catastrophically at $\phi = 41\%$. (*b*) The Lindemann parameter is plotted versus ϕ. The Lindeman parameter, which marks the point at which superheating is no longer observed, is obtained by extrapolating to $\phi_s = 42\%$. (Figure is reproduced with permission from [170]. Copyright 2012 The American Association for the Advancement of Science.)

experiments showed that if a crystal is heated above its melting temperature (e.g. if its packing is reduced below its fluid–crystal transition volume fraction), then thermal fluctuations create small pockets of liquid nuclei. The experimenters found a critical liquid nucleus size above which the liquid nuclei grow; smaller nuclei, however, recrystallize into the solid phase. When a crystal is slightly superheated, nuclei that are larger than the critical size are rare, but, once formed, the supercritical nucleus will grow slowly into the bulk and will initiate melting. In the case of strong superheating, the incubation time becomes much shorter, and multiple supercritical nuclei typically develop and coalesce, significantly accelerating the melting process. It was further discovered that when the packing fraction of the sample was between 0.43 and 0.41, the superheated PNIPAM crystals became unstable and melted catastrophically, as shown in figure 8.

5.3. Melting in 2D

Melting of crystals depends on dimensionality: 2D crystals and 3D crystals melt in significantly different ways. The well-known KTHNY theory [175–178], for example, predicts two-stage melting for a 2D crystal, with an intermediate hexatic phase between crystalline and liquid phases. The hexatic phase maintains quasi-long-range orientational order, while its translational order is short-ranged. 2D PNIPAM colloids have been recently employed to unambiguously reveal this two-stage melting process [49].

By comparison to magnetic particles, which interact via long-ranged dipole–dipole interactions [13, 23, 179], the PNIPAM particle experiments probe melting behavior in a system with short-ranged repulsive interactions. Thus, the PNIPAM experiments demonstrate that liquid–hexatic–crystalline transitions occur in systems with short-range repulsive interparticle potentials. Previously, other colloidal

experiments have employed polystyrene or PMMA particles to study crystal melting in 2D, and although these studies discovered important fundamental effects, they typically required either multiple samples or spatial gradients of some sort within the samples; both scenarios noted above can complicate data analysis and introduce ambiguities [180, 181]. The PNIPAM study by Han *et al* was also the first experimental investigation to employ the order parameter susceptibility to identify phase transitions between the different 'assembled states' during melting. The order parameter susceptibility proved (in these studies) to be a more reliable parameter for phase transition determination than the decay characteristics of correlation functions that are typically used. The latter are often susceptible to finite spatial-window and finite time-window effects.

Specifically, the sample was prepared by loading PNIPAM colloidal suspensions between two coverslips. Bright-field microscopy was employed to image the motion of individual particles at different packing fractions above and below the melting point. By contrast to the pre-melting observed in 3D crystals, 2D crystals were observed to melt homogeneously/simultaneously with no particular preference to defects within. Among other predictions, KTHNY theory suggests that crystalline, hexatic and liquid phases can be distinguished by the different decay behaviors of the orientational order parameter g_6. For example, in the crystalline phase, the spatial correlation of the orientational order parameter $g_6(r)$ is long-ranged (nearly a constant); in the hexatic phase, $g_6(r)$ maintains quasi-long-range order but decays via a power law; in the liquid phase, $g_6(r)$ is short-ranged and decays exponentially. However, the fitting of g_6 to the different functional forms can sometimes be ambiguous, because these data are susceptible to the finite-size and finite-time effects. Thus, in addition to carrying out the more traditional correlation analysis, Han *et al* [49] utilized the fluctuations of the order parameters (i.e. the corresponding order parameter susceptibilities) to quantitatively identify phase transitions during melting of 2D PNIPAM microgel particle monolayers. Importantly, when the sample packing was changed, and the sample evolved from crystalline to hexatic phase, long-range translational correlations were lost, and the corresponding translational order parameter susceptibility, χ_T, was observed to vary substantially and discontinuously across the transition, as shown in figure 9(*b*). On the other hand, the orientational susceptibility stayed approximately constant across the crystal–hexatic transition, and it remained small in the hexatic phase, until the packing fraction for the transition from hexatic to liquid phase was approached; here, a peak in χ_6 was observed, as shown in figure 9(*c*). Thus by using the order parameter fluctuations, Han *et al* very clearly separated the three stages of melting in 2D. In addition, further analysis suggested that two other sub-stages were present in the melting process: a dislocation precursor stage in the crystal before the hexatic phase was reached and a pre-freezing stage in the liquid phase, but more work remains to clarify these effects. In the future, besides directly elucidating melting phenomena, the PNIPAM particle systems can also be utilized *in situ* to study the mechanisms

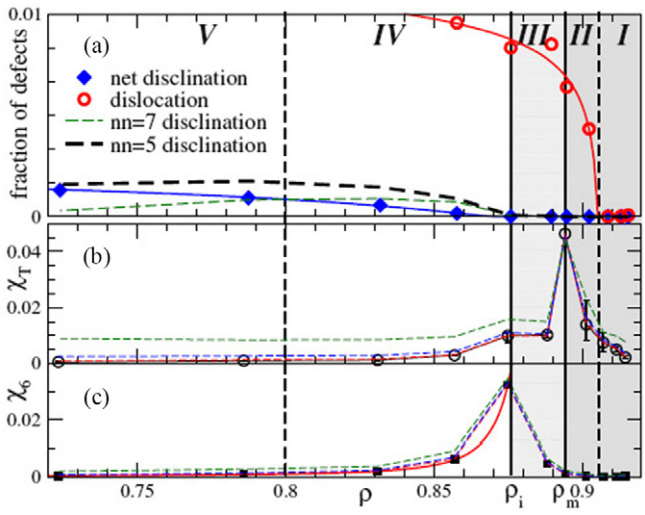

Figure 9. Different stages of melting of the 2D PNIPAM microgel particle systems. (*a*) Defect densities as a function of areal packing fraction. (*b*) Translational and (*c*) orientational susceptibilities as a function of areal packing fraction. (Note, the dashed curves: derived from subbox sizes $L = 5, 10, 20\,\mu$m from top to bottom, and the solid curve is extrapolated to large L.) Vertical solid lines partition crystal regions (I and II), hexatic region (III), and liquid regions (IV and V). Notice that the crystal–hexatic and hexatic–liquid transitions are clearly determined from susceptibilities in (*b*) and (*c*). Region II is a dislocation precursor stage of the crystal. Region IV is a pre-freezing stage of the liquid with some ordered patches. (Figure is reproduced with permission from [49]. Copyright 2008 American Physical Society.)

and dynamics of defect formation and nucleation processes in the 2D short-range repulsive systems.

Additionally, PNIPAM particles were utilized to study crystallization at an air–water interface [324]. Attractive capillary forces and convective flow at the air–water interface lead to controlled growth of large crystalline domains.

5.4. Colloidal crystal films and quasi-2D frustrated systems

Considering the stark differences between 2D and 3D melting, it is natural to ask what happens for film-like suspensions that fall somewhere between pure 2D and 3D limits. In other words, when can a thin multilayer crystal be considered to be a 'bulk' 3D system? To answer this question, Peng *et al* investigated the melting processes of PNIPAM crystals with different numbers of layers [182]. Briefly, the experimenters found that when the number of crystal layers increased from 1 to 2, the hexatic phase was relinquished. Further, for colloidal crystal thin films between 2 and 4 layers, melting was observed to occur from the sample boundaries and from within the sample. Interestingly, a fluid–crystal coexistence region was found in the thin-film phase diagram that increased smoothly in size from approximately zero to the bulk value with increasing layer number. 3D interfacial melting behavior (i.e. bulk-like behavior) was recovered for crystalline films with more than 4 layers.

A different phenomenon was observed when PNIPAM particles were confined in a cell ~1.5 layers thick. In this case, the colloidal particles assembled into a hexagonal

lattice in the transverse plane, but the particles were also able to move slightly out-of-plane perpendicular to the 2D triangular lattice, i.e. the particles were able to buckle out-of-plane. Importantly, a particle at the bottom of the chamber prefers neighbors that reside at the top of the chamber; this preference maximizes the free volume of each neighbor. That is, this type of nearest-neighbor interaction maximizes system entropy and minimizes system free energy. In fact, this type of interaction between neighbors, wherein a 'buckled down' particle wants to neighbor with a 'buckled up' particle, is analogous to the antiferromagnetic interaction between neighboring spins in magnetic systems. It turns out that macroscopic systems such as the particle system we have described, as well as the antiferromagnetically interacting spins on a 2D triangular lattice, are frustrated [183–186]. This frustration can be understood by considering a typical triangle on the 2D triangular lattice; in the lowest energy state, two of the bonds will be satisfied (up–down), but one bond will not be satisfied (up–up or down–down). Superficially, the classic analysis of antiferromagnetic interacting Ising spins on a triangular lattice by Wannier [187] is realized in this classical colloidal system, along with its consequences for a ground state with an exponentially large number of energetically degenerate frustrated states.

Han *et al* studied the structure and dynamics of frustrated PNIPAM systems [50]. Although the idea of frustrated particles in quasi-2D samples cells had been suggested many years ago [17, 180, 190–192], little work was carried out on this problem. The PNIPAM system proved particularly attractive for investigation of these classical frustration phenomena, because it was possible to temperature-tune the ratio of particle diameter to cell thickness and lattice constant. This capability effectively offered the experimenters a way to vary the strength of the antiferromagnetic interaction compared to the thermal energy. The Wannier Ising model solution predicts that 2/3 of particle bonds should connect 'up' and 'down' particles (satisfied), and 1/3 of the particle bonds should connect two 'up' particles or two 'down' particles (frustrated); further, both types of bonds are randomly distributed through the system. However, the colloid experiments found that the 'up' and 'down' particles are not fully random; instead, 'up' or 'down' particles tend to form zig-zag lines, which slightly deformed the underlying lattice and thus increased the packing efficiency. Figure 10 shows the buckled states of confined PNIPAM particles at different packing fractions. The researchers were able to understand the system structure with a model that had frustration, but also included lattice distortion energies [50, 188, 189, 193]. The dynamics of the frustrated colloidal packings were also studied by video microscopy and exhibited glass-like behaviors; the ability to investigate dynamics of these macroscopic particle is also a unique feature of the colloidal systems compared to work done in the hard matter community with model media [186, 194–196]. Thus, the colloidal systems have garnered some recent theoretical interest [197] as a result of their relative advantages for dynamical control and observation.

PNIPAM particles were also confined to narrow glass capillaries [333], which have characteristics of 3D and 1D

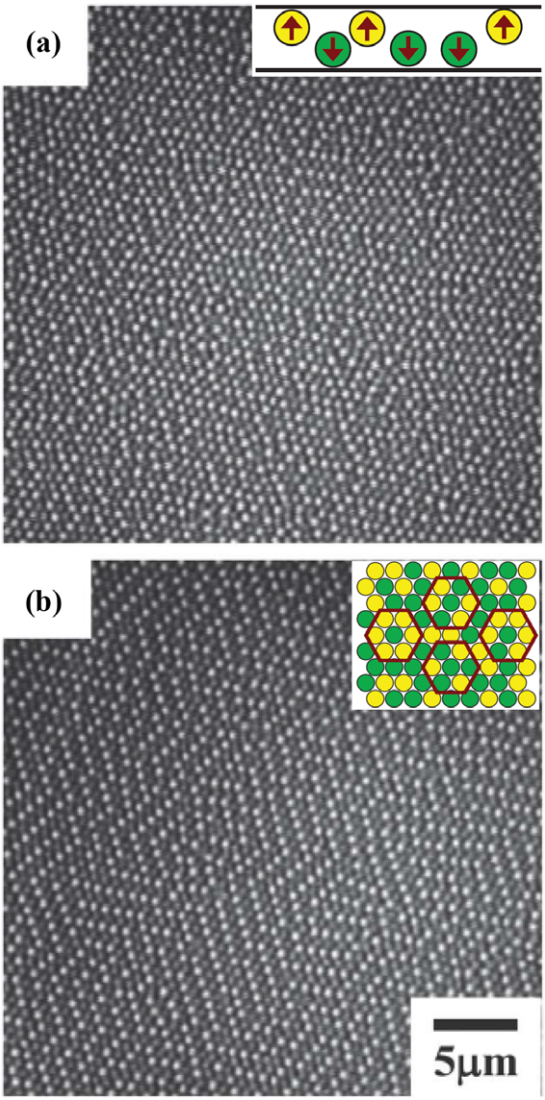

Figure 10. Buckled monolayer of colloidal spheres. Bright spots are particles that buckle 'up' towards the microscope objective and dark spots indicate 'down' particles. (*a*) At $T = 27.1\,^{\circ}\mathrm{C}$, the numbers of 'up' and 'down' particles are roughly the same, and the frustrated and satisfied bonds are randomly distributed. Inset: cartoon showing buckled spheres in side-view. Yellow spheres are near the top of the chamber; green spheres are near the bottom of the chamber. (*b*) At $T = 24.7\,^{\circ}\mathrm{C}$, frustrated bonds form zigzagging strips, which are not predicted by the Ising model, but can be understood if lattice distortions are included in the theory [50, 188, 189]. Inset: cartoon showing hexagonal lattice in top view. (Figure reproduced with permission from [50]. Copyright 2008 Nature Publishing Group.)

(for extreme constraint in two out of three dimensions) systems. When spheres are packed in cylinders of slightly larger diameter, maximal packing is achieved through helical structures with varying degrees of chirality, depending on the exact ratio of sphere diameter to cylinder diameter. By increasing temperature, and thus decreasing packing fraction, PNIPAM particle packings in glass capillaries melt and transition between chiral structures. No discontinuous change in translational order was observed, though evidence of a crossover and coexistence in orientational order is observed. Such a crossover is less reminiscent of the 1D case, which

is predicted to lack phase transitions [332], or the 3D case, which features a single first-order phase transition; instead, it is reminiscent of the orientational-order based hexatic crossovers predicted in 2D packings by KTHNY theory [328–331].

6. Glasses and disordered packings

Arguably, PNIPAM suspensions have proven to be even more useful for the study of disordered solids/glasses than crystalline systems. Glasses are mysterious. If you ask a layperson to describe window glass, they will tell you two things: it is transparent, and it is hard. The transparency of window glass is a result of its wide electronic band gap. However, the exact reasons for why glasses are hard are difficult to ascertain. Further, while ordered systems undergo a sharp transition from liquid to crystal, the transition from liquid to glass is more ambiguous. Compounding these mysteries is the surprising commonality of phenomena observed across a broad spectrum of disordered solids including colloidal suspensions [3], granular media [198, 199], metallic glasses [200, 201] and polymer glasses [202]. Indeed, the fact that systems with such different microscopic constituents behave in qualitatively similar ways has spawned searches for concepts that unify these diverse materials [122, 203, 204].

A few key differences distinguish colloidal glasses and molecular glasses [205]. Notably, molecular glass-formers undergo a transition from liquid to glass when sample temperature is decreased, while colloidal glasses form from the liquid phase when sample packing fraction is increased. Thus, while many similarities between these paths to glass formation exist, the pathways are not identical [205, 206]. Additionally, colloidal particles are inherently polydisperse, while molecules are identical, and polydispersity leads to effects in colloidal systems that are not generally found in molecular systems [207, 208]. Finally, even though particle motions in both molecular and colloidal glasses are driven by thermal fluctuations, the colloidal particles experience damping from the surrounding fluids, an effect that is absent in atomic or molecular glasses.

The study of colloidal glasses, however, offers many advantages. Like the molecular systems, colloidal glasses are thermal, but in contrast to the molecular systems, the motions of individual particles in colloidal glasses can be directly resolved via optical microscopy; analogous real-time observations of rearrangements in molecular glasses are a rarity [209]. Colloidal glass experiments have taken advantage of this single-particle resolution to directly image collective rearrangements and thereby characterize evolving dynamics with respect to aging time or packing fraction [3]. Additionally, the interactions between spherical colloidal particles are simpler than those of molecules, a feature which affords direct comparisons to theory and simulation. Recently, for example, a remarkable colloid experiment measured particle relaxation times that varied over approximately eight orders of magnitude, from 10^{-3} to 10^{5} s, and the experiment uncovered significant deviations from mode-coupling theory predictions [5].

6.1. Soft particles make strong glasses

An interesting recent study probed the effects of particle stiffness on the glass transition using PNIPAM particles. Specifically, suspensions of PNIPAM particles were synthesized with different amounts of polyacrylic acid, thereby producing ensembles of polydisperse particles with varying stiffness at the individual particle level [210]. Then, the particle relaxation time, τ_α, was measured. τ_α is extracted by fitting the intermediate scattering function to a stretched exponential, i.e. $g_1 = \exp(-t/\tau_\alpha)^\beta$; here g_1 is the intermediate scattering function, β is the so-called stretching exponent, and τ_α represents the average time it takes a particle in the glass to move a distance of order its diameter. This parameter was measured via light scattering as a function of scaled particle concentrations (ζ) for soft, intermediate, and stiff microgel particles (figure 11). The scaled particle concentration, ζ, is simply the particle number density multiplied by the volume of an underformed particle. For hard spheres, ζ is identical to volume fraction, and must be less than one. Soft PNIPAM particles are deformable; thus ζ can reach values as large as 10 in these systems. All of the systems undergo a glass transition at a large particle (scaled) concentration, ζ_G. Of course, τ_α is expected to be very large and diverging at the glass transition; in this particular study, large means $\tau_\alpha \approx 100$ s at ζ_G. Interestingly, stiff particles were found to experience dynamic arrest at the lowest particle concentration ($\zeta_G \approx 0.6$); intermediate stiffness particles undergo dynamic arrest at a higher particle concentration ($\zeta_G \approx 7$), and soft particles undergo dynamic arrest at the highest particle concentration ($\zeta_G > 10.0$). Thus, the glass transition in these systems was highly dependent on particle stiffness.

The implications of this stiffness dependence of the glass transition become clear when the data are plotted on the traditional (normalized) Arrhenius plot [211]. By plotting τ_α versus ζ/ζ_G, for example, data from all three particle types can be compared. Soft particles are 'strong' glass-formers, meaning that their relaxation time increases slowly with increasing ζ/ζ_G, i.e. a large increase in concentration is necessary for a strong glass-former to vitrify. Stiff particles are 'fragile' glass-formers, meaning their relaxation time increases rapidly (~exponentially) with increasing ζ/ζ_G, i.e. fragile glass-formers vitrify with a small increase in concentration. Intermediate particles are qualitatively and quantitatively in between the soft and stiff limits. Simulations of collections of interconnected springs have similarly found that networks with smaller spring constants are 'strong' glass-formers while networks with stiffer springs are 'fragile' glass-formers [212]. Further, simulations found that the fragility of glasses composed of soft particles depends on both packing fraction and temperature [206, 212]. If temperature is varied and packing fraction is near the athermal jamming transition packing fraction, for example, then the particle packing behaves as a 'strong' glass-former. On the other hand, if the packing fraction is larger than the athermal jamming transition packing fraction, then the particle packing behaves as a 'fragile' glass-former.

This identification of 'fragile' and 'strong' colloidal glasses represents yet another commonality between colloidal

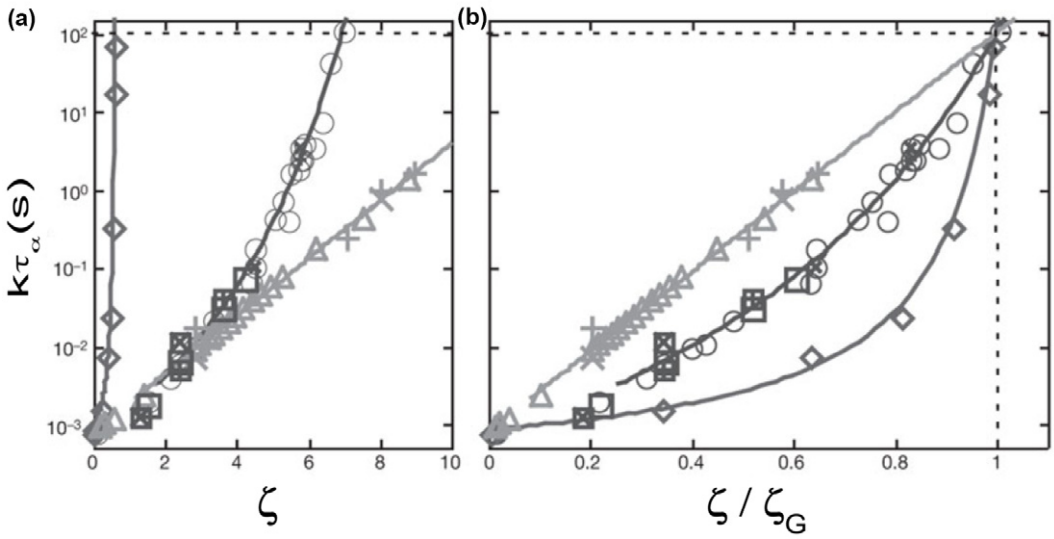

Figure 11. (*a*) Plot of $k\tau_\alpha$, the normalized relaxation time, versus ζ, the scaled particle concentration, for stiff (diamonds, $R_0 = 95$ nm, compressibility ∼0%), intermediate (empty circles, $R_0 = 92$ nm, compressibility ∼15%) and soft (triangles, $R_0 = 80$ nm, compressibility ∼30%) colloidal glasses composed of microgel particles. (*b*) Same as (*a*), with ζ normalized by ζ_G, where ζ_G is the value of ζ when $\tau_\alpha = 100$ s. (Figure is reproduced with permission from [210]. Copyright 2009 Nature Publishing Group.)

glasses and molecular glasses. Thus the PNIPAM particles, with their varying stiffnesses, offer the possibility for experimental study of concepts related to fragility in glasses, i.e. concepts developed originally from study of atomic and molecular systems, with single-particle resolution.

As a technical aside, we note that the use of PNIPAM particles makes comparison of the behavior of a variety of systems near the glass transition relatively easy. The experimental chambers are loaded at small particle concentrations in the liquid phase, and then the system is driven to undergo a glass transition simply by decreasing temperature. Further, data at more than 10 different particle concentrations were required to fully characterize the dependence of τ_α on ζ/ζ_G for each particle type (i.e. particle stiffness). Had the particles not been thermoresponsive, then >30 samples would have been required! In the present study, the data were collected with a total of ∼10 samples.

6.2. Dynamic correlation lengths

The soft nature of PNIPAM particles has been suggested to lead to very long-ranged dynamic correlations in disordered media [213]. This behavior contrasts with collective rearrangements in glasses composed of hard spheres, e.g. PMMA particles, which are typically limited to length scales on the order of a few particle diameters [3, 214]. Duri *et al* recently developed and exploited a novel light scattering technique that enabled particle dynamics to be simultaneously measured in different spatial regions of the sample. Using this method, they found that correlated particle dynamics can extend to macroscopic length scales in suspensions of soft PNIPAM particles [215]. In fact, the largest dynamic correlation lengths that were measured were similar to the size of the system itself. These observations suggest that intrinsic differences exist between disordered packings of soft particles versus hard particles. In the future, PNIPAM particles with different stiffness, e.g. as developed in [210], appear especially well suited for comprehensive exploration of the effects of particle softness on dynamic correlations in glasses.

6.3. Aging

After initial formation, glasses relax via a non-equilibrium process called aging during which their dynamics slow dramatically and become more heterogeneous. These glass dynamics depend on elapsed time from the quench, i.e. the so-called waiting time, t_w. This time dependence is typically captured by the ensemble-averaged particle mean square displacement (MSD) [216]. For glasses, the MSD first grows with increasing correlation time and then plateaus; the MSD plateau corresponds to 'caged' particle behavior. At a still longer correlation time, sometimes called the 'relaxation' time, the MSD experiences an 'upturn' corresponding to some type of cage rearrangement. During aging, this MSD upturn occurs at later and later 'relaxation' times (τ), i.e. as the waiting time, t_w, increases. Typically, the upturn time (τ) increases by many orders of magnitude during aging, until it finally falls outside the experimental measurement time window.

Despite this immense change in dynamics, accompanying structural changes have proven difficult to identify [216–218]. For example, recent colloidal experiments were performed utilizing magnetic stir bars to 'rejuvenate' colloidal glasses [216, 218]. Despite dramatic changes in dynamics, however, these experiments did not discern any change in structure. One limitation of these experiments was that shear from the magnetic stir bar caused particles to drift, even after the stir bar had been turned off. Thus, observations of aging could not occur until after this drifting had ceased. Simulations, on the other hand, aging at an earlier times, e.g. shortly after the sample is rejuvenated, should be accompanied by measureable structural changes (e.g. [217]).

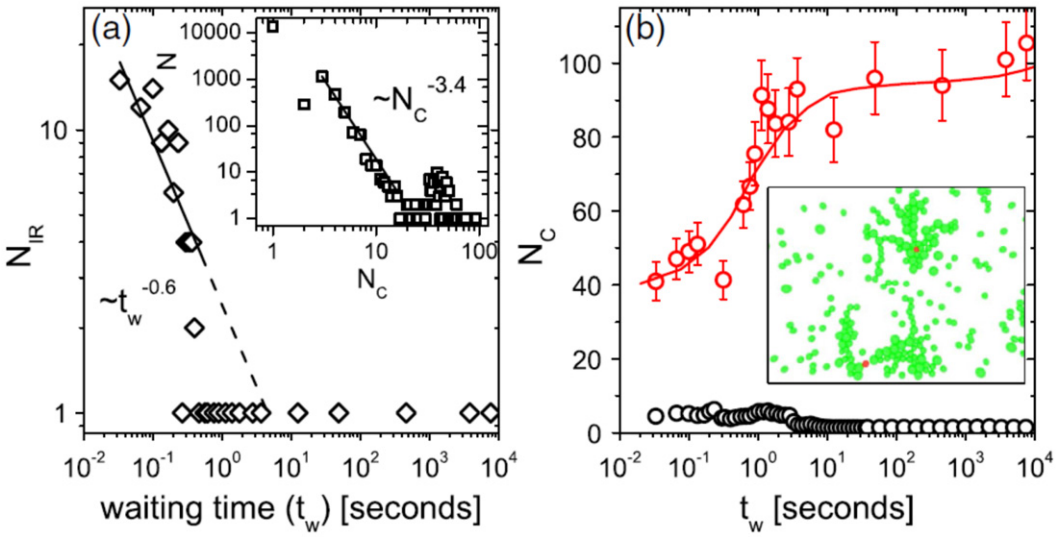

Figure 12. (*a*) N_{IR}, the number of IRs, versus t_w. The line is a power law fit. Inset: histogram of N_C, fast particle cluster sizes, for $0.03 \leqslant t_w \leqslant 3$ s. The line is a power law fit. (*b*) Average number of fast particles per cluster for all clusters (black circles) and the average number of fast particles per cluster for only clusters containing a particle undergoing an IR (red circles), versus t_w. The line guides the eye. Inset: snapshot of the 10% fastest particles at $t_w = 0.62$ s, featuring two large clusters. Particles that irreversibly rearrange are plotted in red. (Figure reproduced with permission from [219]. Copyright 2009 American Physical Society.)

In this spirit, clever usage of PNIPAM particle suspensions can permit observation of aging very shortly after a rapid temperature quench [219–221]. In [219], rapid optical heating and cooling schemes are employed to manipulate PNIPAM colloids from solid to liquid, and then to glass phases. Specifically, a small amount of red dye is dispersed in a 'solid' packed suspension of temperature-sensitive microgel particles; a central portion of the sample is then illuminated with light from a mercury lamp. The red dye preferentially absorbs the lamp light, relaxes non-radiatively, and in the process it increases the temperature of the central portion of the suspension. This temperature increase melts the colloidal solid into the liquid phase. After allowing particles to rearrange in the liquid phase, the illuminating lamp light is turned off. Because the microscope and the vast majority of the sample remain at their original low temperature, the excess heat dissipates rapidly (<0.1 s), and the suspension is quickly quenched into the glass state. At this time, aging begins, and the observation window begins as well.

Constituent particles in glasses tend to rearrange in a correlated manner involving many neighbors [3, 222–224], making it difficult to determine which particle configuration was initially unstable by use of MSDs [225, 226]. What is the nature of these rearrangement events and how do they change with time during aging? In simulations, it was observed that if a motional event causes a particle to lose four of its nearest neighbors, then the particle rarely recovers its initial configuration, i.e. it has undergone an *irreversible rearrangement* (IR) [227]. These so-defined IRs facilitate differentiation between affine motions that maintain local structural configurations, and non-affine motions that contribute to relaxation (and dissipation). The PNIPAM experiments outlined above employed video microscopy to track particles within the experimental time window [219], and the experiments discovered that those particles that lose three nearest neighbors never regain their original configuration (i.e. at least over the timescale of the experiment). Thus these particles experience a so-called IR. But the experiments revealed even more information about the aging process.

To study the variation in correlated rearrangements with t_w, the number of IR events occurring in the experiment observational time window was measured as a function of t_w (figure 12(*a*)). The rate of IRs is initially high; ~90 events occur when $t_w < 0.4$ s. However, thereafter the rate slowed dramatically, and only ~15 events occurred over the rest of the experiment. Next, in order to identify clusters of rearranging particles, particles that moved much farther than average were identified, i.e. the 10% fastest moving particles, and clusters of these fast particles were identified by connecting nearest-neighbor pairings of the 'fast' particles [3, 228, 229]. Surprisingly, the average number of particles per fast cluster actually *decreased* from ~5 particles immediately after the quench, to ~2 particles at $t_w = 10\,000$ s (figures 12(*b*)). This result is somewhat counter-intuitive, as previous simulations reported a dynamic length scale that grew during aging [230].

However, closer inspection of the data revealed that some very large clusters exist, some of which contain ~100 particles (figure 12(*a*), inset). Interestingly, it was found that most of these large clusters contained a particle that had undergone an IR. A snapshot of the 10% fastest particles, featuring two such large clusters, is shown in the inset of figure 12(*b*). Next, the average size of these particular clusters of fast particles, all of which contain a particle that underwent an IR, was calculated. The results are plotted in figure 12(*b*). Notice that the average size of these clusters *increases* from ~40 particles just after the quench, to ~100 particles at $t_w = 10\,000$ s; the radius of gyration of these clusters correspondingly increases from ~2.5 to ~4.5 μm. In other words, as the glass ages, more particles must move for IRs to occur.

The observation that clusters of fast moving particles are dramatically larger *when an IR is involved* demonstrates an intimate connection between IRs and dynamic heterogeneity. This effect is reminiscent of the Adam and Gibbs hypothesis, which states that as the glass transition is approached, the number of correlated particles involved in a rearrangement increases [223, 231]. In the present case, the number of correlated fast particles involved in an IR event increases with aging. Rearrangements thus become progressively more difficult to achieve, leading to slow glass dynamics and kinetic arrest.

PNIPAM particles were also utilized recently to study aging glasses in 3D samples [221, 323]. These experiments [221] followed the dynamics of isolated tracer particles and observed spatially heterogeneous dynamics. Additionally, the time to fully age was found to be highly dependent on the amplitude of the quench; larger quench amplitudes lead to faster aging. Rheology experiments [323] found that particle softness affected the glass transition, but did not qualitatively affect aging behaviour.

Finally, recent experiments have employed scattering to investigate the dynamics of aging in rapidly quenched PNIPAM glasses as a function of quench amplitude and history [220, 319]. These experiments facilitated direct comparisons to aging experiments performed with molecular glasses [232]. All of the signatures of molecular glass aging were observed in the colloidal experiments, albeit in qualitatively distinct ways. For example, memory effects were studied by quenching one sample from $T = 32.0\,^{\circ}\mathrm{C}$ to $T = 31.5\,^{\circ}\mathrm{C}$. At the final temperature, the packing fraction decreased as the glass aged. A second sample's temperature was lowered from $T = 32.0\,^{\circ}\mathrm{C}$ to $T = 31.2\,^{\circ}\mathrm{C}$ for 120 s before it was increased to a final $T = 31.5\,^{\circ}\mathrm{C}$. At the final temperature, packing fraction initially *increases*, until it reaches a maximum; at that point, it decreases. However, unlike molecular glasses, this phenomenon did not exhibit an observable dependence on the quench amplitude. Thus, it is becoming clear that although colloidal glasses can capture much of the behavior of molecular glasses, their behaviors can also differ in interesting ways.

6.4. Crystal-to-glass transitions

Disorder plays a critical role in traditional melting and freezing phenomena and in the formation of glasses. Melting from crystal-to-fluid, for example, is a sharp transition accompanied by loss of orientational and translational order and by a dramatic decrease in flow resistance and rearrangement timescale [176]. By contrast, orientational and translational order do not change significantly at the liquid-to-glass transition, even as viscosity and rearrangement timescales diverge [235]. However, frozen-in residual disorder is critical for glass formation. An interesting, less studied but closely related problem [16, 207, 208, 236–243] concerns the role played by frustration and disorder in driving the transformation of a crystal to a glass. Recent experiments with PNIPAM particles explored this transition, from crystalline solid to glass as a function of quenched disorder in both 2D [234] and 3D [233]. The resultant glassy phases acquire typical properties such as dynamic heterogeneity [3, 224, 242, 243] and disorder, but the crystal-to-glass transition is quite sharp, exhibiting features often associated with melting.

The 2D experiments employed bi-disperse PNIPAM particle suspensions with varying small-particle number fractions, n_S (i.e. $n_S = 0.00$–0.50). By adjusting the sample temperature, the area fraction, ϕ_A, was readily increased from $\phi_A \approx 0.75$ to $\phi_A \approx 0.90$ with a step size of $\sim$0.01 in ϕ_A. Thus, $\sim$100 combinations of n_S and ϕ_A were produced from $\sim$8 samples. Again, the substantial technical advantage of using PNIPAM particles should be emphasized: with traditional (non-temperature sensitive) particles, the same investigation would have required $\sim$100 different samples!

The structural correlations associated with orientational order and the dynamic correlations associated with particle rearrangements were both measured by video microscopy. The path from crystal to glass was experimentally found to be marked by a sharp drop in structural correlations and a sudden jump in dynamical correlations. The crystal–glass transition therefore bears structural signatures similar to the crystal–fluid transition [49, 176]: the orientational order correlation function, g_6, changes form quite abruptly from quasi-long range to short range at the transition point; the orientational order susceptibility, χ_6, exhibits a maximum at the transition point; and the number of free disclinations, defects associated with the liquid state, increases. These changes are all reminiscent of crystal–liquid phase behavior [49, 176], suggesting a distinct transition from crystal-to-glass via increasing quenched disorder [240, 241]. Thus, this result stands in contrast to the transition from liquid to glass, wherein changes in structural correlations are not observed [235]. Recent experiments performed in 3D also observed a sharp transition from an ordered crystalline phase to a disordered glassy phase [233]. A similarly sharp transition from homogeneous to heterogeneous *dynamics* was observed to accompany these structural changes. In particular, domains of correlated particle rearrangements (i.e. dynamic heterogeneity) appear to turn-on suddenly. This so-called dynamic heterogeneity is characterized by temporal fluctuations in the two-time overlap correlation function [244], Q_2: $Q_2(d_L, \Delta t) = \frac{1}{N_{tot}} \sum_{i=1}^{N_{tot}} \exp(-\frac{\Delta r_i^2}{2d_L^2})$ [24]. Here d_L is a pre-selected length scale to be probed and Δr_i is the distance particle i moves in time Δt. If a particle moves a distance smaller than d_L, Q_2 will be close to 1; if a particle moves a distance greater than d_L, Q_2 will be close to 0. These fluctuations are commonly quantified by their variance, the dynamic susceptibility [199, 224, 244] χ_4, which is a function of the length scale, d_L, and timescale, Δt.

Rather than selecting arbitrary length and time scales, χ_4 is calculated in [234] for all relevant values of d_L and Δt. The maximum value of χ_4 (i.e. χ_4^*) is plotted in figure 13(*b*) for each n_S at $\phi_A = 0.85$. In crystalline suspensions, χ_4^* is small ($\sim$1). Once n_S is increased beyond 0.02, however, χ_4^* jumps (almost) discontinuously to $\sim$35. As n_S is increased still further, χ_4^* remains fairly constant. This sharp change is absent in the liquid–glass transition [199, 224]. For comparison, χ_4^* increases continuously as packing fraction is increased across the liquid–glass (figure 13(*c*)) transition, similar to

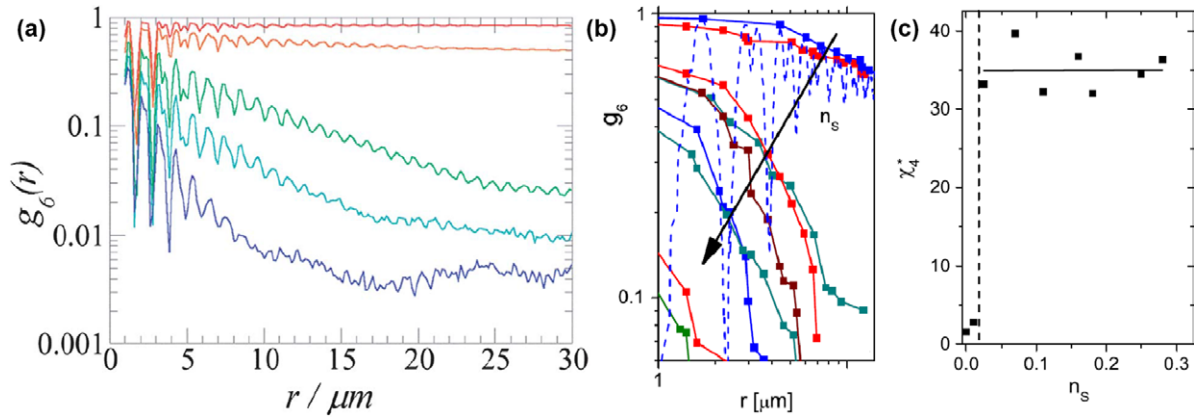

Figure 13. Orientational order correlation function, g_6, as a function of interparticle distance, r, is shown for 3D (a) and 2D (b) experiments with different fractions of dopant particles. (c) The maximum value of χ_4, χ_4^*, plotted versus the fraction of small particles, n_S. The solid line is a linear fit, to guide the eye. The dashed line marks $n_S = 0.02$. (Figure is reproduced with permission from [233] (a) (Copyright 2013 Royal Society of Chemistry) and [234] (b) and (c) (Copyright 2010 American Physical Society.)

[199, 224]. Thus, while the liquid-to-glass transition is somewhat ambiguous and often difficult to define, the crystal-to-glass transition with increasing quenched disorder appears sharp and unambiguously defined.

As noted above, a similar experiment was performed in three dimensions [233]. Despite the change in dimensionality, a similarly sharp transition is observed from ordered to disordered phases. Thus, the crystal-to-glass transition appears to be independent of the exact nature of the fluid-to-crystal transition.

Finally, highly charged PNIPAM particles with long-range interparticle repulsion are potentially excellent model systems to study the influence of frustration and packing fraction on the crystallization of monodisperse colloidal suspensions. Recent light scattering studies of this system class show a transition from homogeneous to heterogeneous nucleation to finally stable glasses with increasing packing fraction [316]. Clearly, the PNIPAM system appears to be an excellent model system in many guises for study of the relationship between structural order and dynamics (e.g. dynamic heterogeneity) in glassy systems.

6.5. Glass–liquid–gel

PNIPAM particles have been used to investigate disordered gel phases [245, 320]. PNIPAM particles are purely repulsive for temperatures below the LCST of $T \approx 33\,^{\circ}$C. Conversely, for temperatures above the LCST, PNIPAM particles can experience an interparticle attraction.

Unlike most of the experiments discussed thus far in this review, Romeo *et al* [245] explored the mechanical behavior of packings of PNIPAM particles at temperatures above and below the LCST (figure 14). Below the LCST, they found their polydisperse particles formed a glass. As they increased the temperature (still below the LCST), the glass melted and became a fluid. Interestingly, at temperatures above the LCST, interparticle attractions lead to the formation of a solid–gel phase. Thus, by increasing temperature, a single sample was observed to transition from a dense glass phase, to a dilute liquid phase, and then to a percolating gel phase.

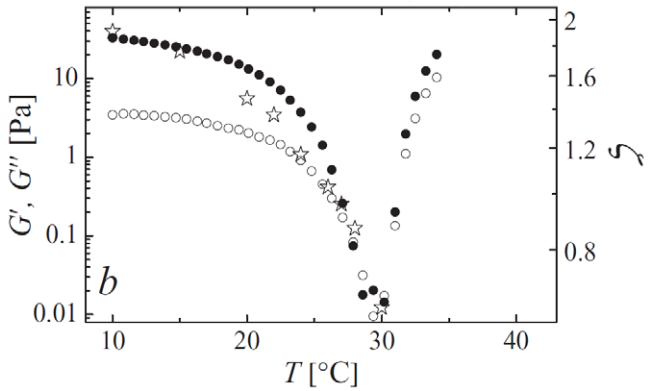

Figure 14. Temperature dependence of the linear viscoelastic moduli G' (solid circles) and G'' (open circles), and particle volume fraction ζ as obtained by viscosity measurements (stars). (Figure reproduced with permission from [245]. Copyright 2010 Wiley.)

6.6. Jamming

The packing fraction control available to PNIAPM colloids is particularly well suited for studies of jammed systems, because many of the predictions of jamming theory involve scaling effects as a function of packing fraction near the jamming point. Briefly, liquid–solid structural arrest occurs in a broad array of disordered systems, including atomic/molecular [211], polymer [246] and colloidal glasses [3] and granular media [199]. These disordered systems are different in many ways, but their phenomenology exhibits a surprising amount of commonality. Relatively recently, Liu and Nagel proposed a novel theoretical scheme to unify the description of the behavior of jammed systems [122]. In particular, they proposed a conceptual phase diagram for the jamming transition which separates jammed (solid) states from unjammed (fluid) states; the diagram is shown schematically in figure 15). The axes of this phase diagram are temperature, stress and inverse density (i.e. the reciprocal of volume fraction). The description can therefore be applied to equilibrium and non-equilibrium systems. In fact, the description attempts to unify a wide range of structural arrest

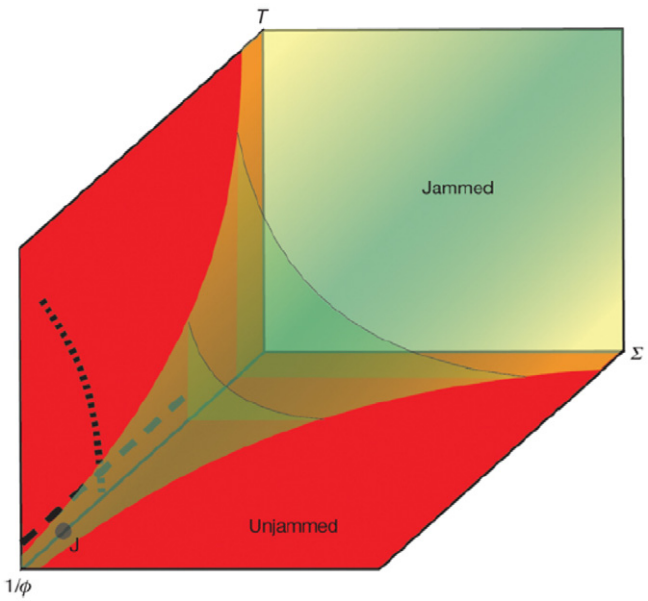

Figure 15. The surface of the green region in the 3D space defined by temperature T, inverse packing fraction $1/\phi$ and applied stress corresponds to the dynamical glass transition; within the green region the system is out of equilibrium [122]. The point marked J represents a phase transition occurs as ϕ is increased while $T = 0$ and $= 0$. In the experiments, we varied the packing fraction at nearly fixed temperature, along the horizontal dashed line. In the simulations, packing fraction is varied at fixed temperature along the horizontal dashed line, and temperature is varied at fixed pressure along the dotted curve. (Figure reproduced with permission from [132]. Copyright 2009 Nature Publishing Group.)

phenomena (including glass formation). Jammed states form in some regions of the diagram, e.g. where density is high, and/or temperature and applied stress are low [122].

The term 'jamming' is sometimes used loosely to refer to different physical scenarios. Strictly speaking, the jamming transition is defined for athermal systems; at $T = 0$, the jamming transition is a 'phase' change that occurs at a critical packing fraction (i.e. at the so-called J-point), near which various scaling laws are predicted [122–124, 156]. For thermal systems, i.e. $T > 0$, the term jamming transition is sometimes used to refer to the so-called dynamic glass transition, e.g. the point at which the particle relaxation timescales exceed an arbitrary threshold of ≈100 s. We note that while many experiments and simulations of thermal systems have observed phenomena reminiscent of the athermal jamming transition [132, 134, 247], some controversy about the assignment of 'jamming' to these phenomena exists and is debated in the community [129, 163]. In particular, the existence and the physical interpretation of a temperature T^*, below which a jamming-like transition must be expected, is widely discussed [129, 163, 248].

6.6.1. Structural signatures of jamming. In the colloidal realm, with notable exceptions (e.g. measurements by Trappe *et al* [19]), relatively few experiments have tested theoretical jamming concepts. Thermoresponsive PNIPAM microgel particles are changing this situation. One recent set of experiments [132], for example, set out to probe predictions about the jamming transition. The experiments employed binary mixtures of PNIPAM particles in 2D (i.e. the particles were confined between two glass slides). Samples were temperature-tuned so that their volume fraction varied above and below the jamming point. Imaging and particle tracking were thus carried out via bright-field microscopy over many different packing fractions, ranging from $\phi = 0.76$ to $\phi = 0.93$.

Measurements of particle MSD near the jamming point exhibited classic glass-like behavior [3, 249]. Further, other parameters such as the dynamic susceptibility also exhibited pronounced peaks at the jamming point. Perhaps more importantly, the pair-correlation function, $g(r)$, of the larger particles, was shown to exhibit a structural signature of the jamming point for the first time [124]. Specifically, the height of the first peak of the pair-correlation function, called g_1, increased at the lower packing fractions from $\phi = 0.76$, reached a maximum value at $\phi \approx 0.84$, and then decreased as ϕ increased further (figure 16). Importantly, this peak in g_1 was reminiscent of the divergence of g_1 observed in athermal simulations of jamming [250]. In fact, accompanying simulations in the paper demonstrated that the divergence of g_1 observed in athermal simulations becomes a sharp peak in thermal systems, which broadens as temperature increases.

Since these initial studies, similar structural signatures of jamming have also been recently reported in 3D PNIPAM suspensions [247, 322] and in granular media [134]. There has also been some theoretical debate about whether the colloid measurement of a maximum in g_1 is truly a remnant of jamming, or whether it is another feature of thermally disordered media [163]. Resolution of this debate may ultimately depend on the softness of the particle interaction potential compared to thermal energies, but regardless, the experiments in both 2D and 3D (and future studies) provide useful data for this ongoing discussion.

6.6.2. Microfluidic rheology near the jamming point. The study by Zhang *et al* discussed above focused on two of three axes on the jamming phase diagram (figure 15), specifically, packing fraction and temperature [124]. Recent work with PNIPAM particles has focused on the third axis: applied stress. In traditional suspension rheology experiments, the suspension transitions from fluid-like behavior to solid-like behavior as the packing fraction of spheres increases near a critical value ϕ_c. Above ϕ_c the system develops a non-zero yield stress and can be considered to be a solid. Theoretical studies have predicted distinctive rheological scaling behaviors for these systems near this critical volume fraction [127, 159, 251]. However, suspensions composed of hard-sphere-like particles are generally unable to explore packing fractions far above ϕ_c. Thus, once again the PNIPAM particles provide an attractive platform to explore physics phenomenology near structural arrest.

Recently, Nordstrom *et al* employed microfluidic channels to study the rheology of PNIPAM suspensions as a function of packing fraction [133]. The experiment was performed in a microfluidic channel 25 μm wide, 100 μm deep and 2 cm long. PNIPAM suspensions were driven through

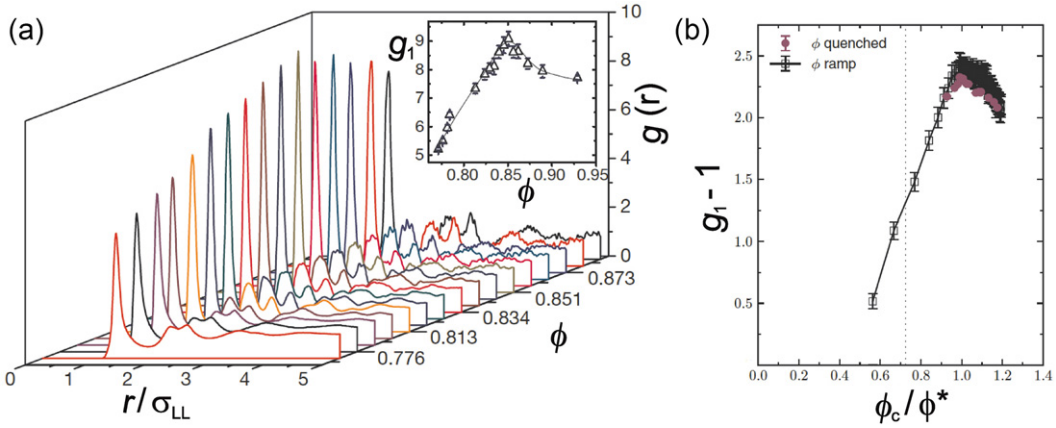

Figure 16. (*a*) Pair-correlation function, $g(r)$, plotted versus interparticle separation, r, as a function of area fraction, ϕ, for 2D experiments. Inset: the height of the first peak in $g(r)$, g_1, plotted versus ϕ. g_1 is peaked at the jamming transition packing fraction. (*b*) $g_1 - 1$, plotted versus ϕ for 3D experiments. Data from fast (quench) and slow (ramp) cooling rates are shown. (Figure reproduced with permission from [132] (*a*) (Copyright 2009 Nature Publishing Group) and [247] (*b*) Copyright 2013 American Physical Society.)

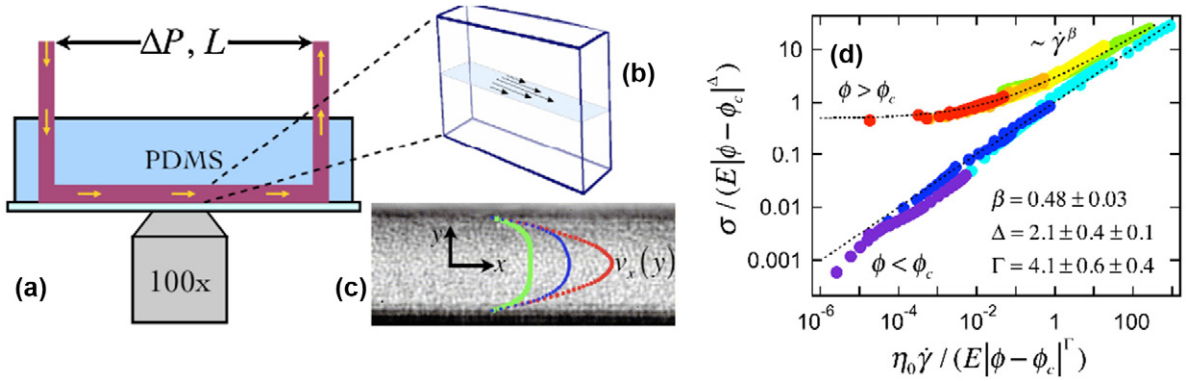

Figure 17. Rheological measurements in microfluidic channels. (*a*) The flow is driven by compressed air through the channel. (*b*) Microscope objective is focused at the middle plane of the channel. (*c*) A video microscopy image of the colloidal flow, colored curves are the velocity profile of a Newtonian fluid (red), PNIPAM samples at $\phi = 0.56$ (blue) and $\phi = 0.64$ (green). (*d*) Collapse of stress and strain rate using critical exponents and . The dashed lines are fits to Herschel–Bulkley form $\sigma = \sigma_y + K\dot{\gamma}^\beta$. (Figures reproduced with permission from [133]. Copyright 2010 American Physical Society.)

the channel by pressurized air as shown in figure 17. High-speed video microscopy was then used to image the particle flow. Local stress σ and strain rate $\dot{\gamma}$ were readily extracted from the experimental pressure drop and variation in particle velocity with position in the channel as measured by particle image velocimetry (PIV) analysis. By controlling sample temperature, the flow of PNIPAM particles in the channel was measured both below and far above the jamming transition. Importantly, these microfluidic rheology measurements facilitated generation of high strain rates while keeping the Reynolds number low (a technically challenging task in traditional rheometers); further, the approach derives results for multiple strain rates in a single measurement.

The resulting collection of microfluidic rheology data is plotted in a suggestive manner in figure 17(*d*). When rescaled by $\phi - \phi_c$, the measured shear stress and strain rate of PNIPAM suspensions at different packing fractions can be collapsed onto two master curves with universal scaling exponents, in agreement with theoretical predictions [127, 251]. The observed scaling behavior supports the notion that, despite its non-equilibrium nature, rheological behavior of dense colloidal suspensions near the jamming transition has some critical point character.

These issues are far from settled. Recent simulations by Ikeda *et al* [154, 155] suggest that two distinct transitions in rheological experiments of soft colloidal suspensions might exist, which they refer to as 'thermal' glass transitions and 'athermal' jamming transitions. This work also raised interesting questions about which transition is probed in typical rheological experiments. In particular, their simulations suggest that the transition observed depends mainly on the experimental temperature and the particle softness. For example, soft particles at high temperature show a glass transition with yield stresses of the order $k_B T/d^3$ at strain rates with associated Peclet numbers, $Pe \leqslant 1$; by contrast, hard particles at lower temperature show predominantly jamming transitions with yield stresses that are orders of magnitude larger at strain rates with associated Peclet number, $Pe > 1$. Recent rheometer-based experiments with PNIPAM suspensions have begun to explore these issues [137].

Interestingly, the PNIPAM particle's Young's modulus E [68] and size suggest that the transition in figure 17 is indeed

a jamming (non-thermal) transition. On the other hand, other rheological experiments on PNIPAM [117] or PS-PNIPAM core–shell particles [116] appear to better described as a glass (thermal) transition. In principle, it might even be possible to prepare PNIPAM systems with intermediate softness that exhibit both transitions in the same sample at different shear rates. This work remains for the future.

7. Phonon modes

From the research described up to this section, it should be apparent that, PNIPAM colloids have been creatively employed to learn about the properties, phase behaviors, dynamics and structure of a plethora of crystals, glasses and related complex fluids. In this section we focus on a different and recent 'hot topic' in the field, namely the measurement of phonon modes in colloidal media. Phonons tell us about the collective vibrations of atoms in solids. Phonon properties and behaviors also help us to understand many of the thermodynamic and mechanical properties of materials, e.g. heat capacity, speed of sound, shear and bulk modulus, etc.

Recent technical and conceptual advances have enabled experimenters to derive phonon modes in dense colloidal systems from the displacement correlations of particles in the samples. These advances, in turn, have revealed novel features of the phonon density of states in glasses and crystals, and have facilitated the experimental discovery of connections between particular phonon modes (i.e. soft and quasi-localized) and particle rearrangements. While PNIPAM colloids have not been employed in all of these recent phonon experiments, they were utilized in much of the seminal research, because of the exquisite sample control they offer (via temperature). For example, the PNIPAM colloids have enabled experimenters to correlate phonon properties with packing fraction near the jamming/glass transition.

The theoretical concept underlying these technical developments is displacement covariance analysis. When the packing fraction of a colloidal sample is sufficiently high, particle diffusion becomes very slow, and the time between rearrangements becomes long. In this case, the system is in a quasi-stable configuration, with each particle moving about an equilibrium position; collectively, the system rests at the bottom of a multi-dimensional potential well. Thermal fluctuations, of course, displace particles from their equilibrium positions producing an increase of system potential energy (see figure 18). The curvature of the potential energy landscape can be mapped out by sampling large numbers of particle configurations displaced from equilibrium. In practice, one constructs a matrix of time-averaged displacement covariance between particles, C, with

$$C_{ij} = \left\langle u_i(t) u_j(t) \right\rangle_t . \tag{1}$$

Here, $u_i(t)$ is the displacement of the particle i at time t from its equilibrium position. The indices $i, j = 1, \ldots, \mathrm{d}N$ run over particles and coordinate directions, N is the number of particles in the field of view, d is the dimensionality of

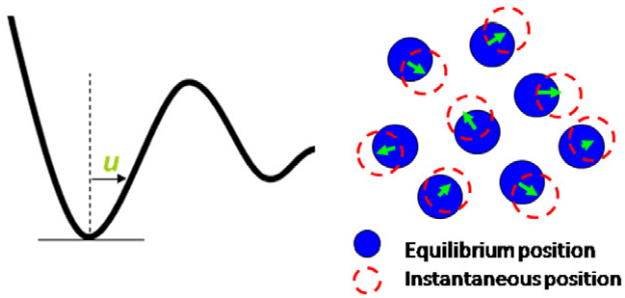

Figure 18. Colloidal samples with stable equilibrium positions rest at the bottom of a potential well. $\boldsymbol{u}$ is the system displacement, arrows represent displacement components on each particle.

the system, and the average runs over time frames. The covariance matrix C, is directly related to the sample stiffness matrix, K, defined as the matrix of second derivatives of the effective pair interaction potential with respect to particle displacements. To the quadratic order, the effective potential energy of the system is $V = \frac{1}{2}\boldsymbol{u}^{\mathrm{T}} K \boldsymbol{u}$. Within the energy basin, the system is assumed thermally equilibrated, and one can then readily calculate various correlation functions from the partition function, $Z \propto \int D\boldsymbol{u} \exp(-\frac{1}{2}\beta \boldsymbol{u}^{\mathrm{T}} K \boldsymbol{u})$, where $\beta = 1/k_{\mathrm{B}}T$. In particular, $u_i u_j\rangle = k_{\mathrm{B}}T(K^{-1})_{ij}$, where indices i and j run over all particles and unit directions. Phonon modes are obtained by diagonalizing the dynamical matrix

$$D_{ij} = \frac{K_{ij}}{\sqrt{m_i m_j}} = \frac{k_{\mathrm{B}}T(C^{-1})_{ij}}{\sqrt{m_i m_j}}, \tag{2}$$

where m_i and m_j are the masses of particles i and j, respectively.

To summarize, the displacement covariance matrix analysis utilizes experimental 'snapshots' of the particle configurations to derive the phonons of the so-called shadow system of particles equilibrated in the same configuration and with the same interactions as the measured colloid, but absent damping. That is, by contrast to the particles in the colloidal suspensions whose motion is strongly damped, the virtual particles of the shadow system are undamped. Nevertheless, the real and shadow systems are characterized by the same correlation and stiffness matrices, because these are static equilibrium quantities. For the shadow system, the stiffness matrix is directly related to the dynamical matrix whose eigenvectors correspond to the vibrational modes and whose eigenvalues correspond to mode frequency. Thus, the covariance matrix analysis permits direct comparison of damped colloidal solids to atomic/molecular solids and to idealized sphere packings.

Several requirements need to be met in the experiments for the covariance matrix analysis to work. First, the system needs to have a stable equilibrium configuration; changes in particle equilibrium positions will produce changes in the collective energy minimum during the course of the experiment, and the assumption that the system rests at the bottom of a potential well will be violated. This requirement is usually met if the particle MSD is flat during the experimental time window. The second requirement is that displacements in a single 'snapshot' are effectively measured at the same time for all particles,

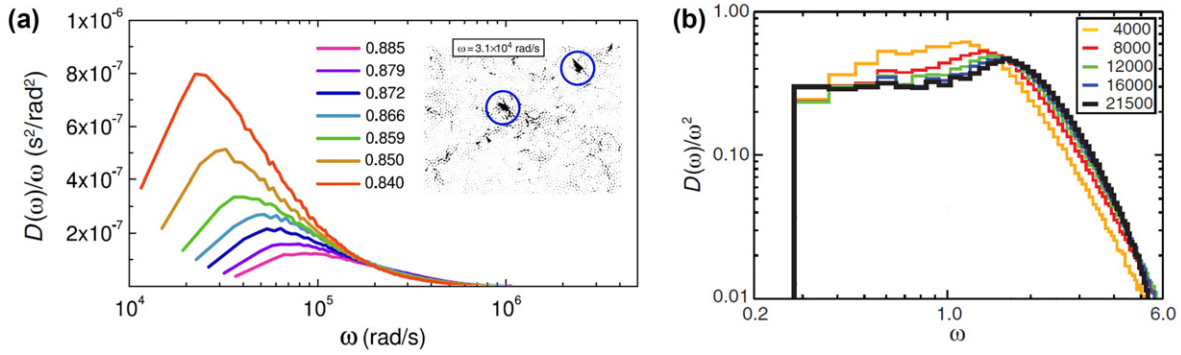

Figure 19. The vibrational density of states, $D(\omega)$, normalized by Debye law predictions, for a 2D disordered glass (a), and a 3D crystal. In each case, the peak suggests the presence of the boson peak. The inset in (a) shows the polarization vector, i.e. the displacements, of each particle for a localized low-frequency mode. In (a), different color lines represent different packing fractions with red as the lowest and pink as the highest. In (b), different color lines were calculated with different numbers of frames (shown in inset). The frequency in (b) is unitless; it is normalized such that $\omega = \sqrt{\lambda \mathrm{MSD}/k_\mathrm{B}T}$, where λ is the eigenvalue of the dynamical matrix, MSD is the particle mean square displacement, k_B is the Boltzmann constant and T is temperature. (The figures are reproduced with permission from [67] (a) (Copyright 2007 American Physical Society) and [252] (b) (Copyright 2010 The American Association for the Advancement of Science).)

and thus each displacement vector $\boldsymbol{u}(t)$ represents one unique configuration of the system. This requirement can be satisfied by employing a rapid shutter (e.g. a camera shutter) over the full field of view in the image acquisition devices.

The quality of the data statistics is also critical for extraction of correct vibrational modes from the measured particle displacements. At a minimum, the number of snapshots, T, used to construct the covariance matrix must be no less than the number of degrees of freedom of the observed system dN [253]. A good measure of the experimental statistics is $R = dN/T$. In practice, larger values of R affect the accuracy of the high-frequency modes more than the low-frequency modes. To fully recover the whole spectrum, values of R less than 0.005 are desirable; for a system of 3000 particles moving in 2D, one requires more than 1 million snapshots to satisfy this criteria. The requirement is often beyond the capacity of many microscopy experiments. Fortunately, this difficulty can be ameliorated by a simple extrapolation operation. In particular, it was recently demonstrated empirically from simulation and in experiment that the eigenfrequencies extracted from different R converge to the $R = 0$ case linearly with R [254]. An experimenter can therefore measure eigenfrequency for different values of R, and then correct the results by linear extrapolation. Besides statistics, care must also be taken when interpreting vibrational modes obtained from experiment with a limited field of view [255, 256].

The first PNIPAM experiments to exploit the covariance method to measure phonons were carried out in 3D colloidal crystals by Kaya *et al* [252]. In their investigation, bright-field microscopy was employed to image a single layer of particles within the full 3D PNIPAM crystal. The experiment by Kaya *et al* observed an excess number of phonon modes above the predictions of traditional Debye theory at relatively low frequencies; this feature is sometimes called a Boson peak in the phonon density of states (figure 19). Their observations suggested that the colloidal crystal has some glassy features which they attributed to particle size and stiffness polydispersity. The authors suggested that such heterogeneities can introduce disorder into the crystal from which glassy behavior can emerge.

The displacement covariance matrix analysis was also tested in 2D PNIPAM crystals [254]. Debye scaling and van Hove singularities characteristic of 2D crystals were observed, thus providing evidence this method is valid for overdamped colloidal packings.

Very recently, Still *et al* derived the elastic moduli of PNIPAM colloidal glasses at different packing fractions starting from the covariance matrix analysis. An interesting result is that in such systems, interparticle friction becomes important and must be taken into account when experiments are compared to jamming theory [317].

The covariance matrix analysis can of course be readily applied to other disordered colloids, besides those made from PNIPAM. Ghosh *et al* [257], for example, studied phonon modes in hard-sphere glasses. In this case, laser scanning confocal microscopy was employed to follow the particles in 3D, and the resultant data was employed to derive phonon modes and density of states via application of covariance matrix methods to single (monolayer) slices of colloidal particles within the full 3D disordered solid of PMMA particles; this team also reported deviations from Debye theory expected for glasses. Further, phonon modes were also studied in 2D glasses composed of hard anisotropic (ellipsoidal) particles [258].

Finally, in a closely related vein, Chen *et al* studied the evolution of phonons and phonon density of states in 2D PNIPAM colloidal glasses [67]. Use of PNIPAM particles enabled *in situ* tuning of sample packing fraction near the glass/jamming transition. This feature has turned out to be particularly important for studying the disordered solids, because it permits experimenters to study physical features of the glass (e.g. the Boson peak) as a function of packing fraction above the jamming point (or, alternatively, above the point at which the solid is fluidized). A second feature of the work distinguished this experiment from those that measured single slices of particles within a 3D sample, i.e. [252, 257]. The use of a true 2D monolayer of particles effectively eliminated

a whole host of ambiguities that arise when one attempts to draw conclusions about the phonons in a 3D sample using data taken from a 2D slice [253, 255, 259, 260]. In the work of Chen *et al* [67], a binary mixture of PNIPAM particles with diameter ratio ≈1.4 (to frustrate crystallization) was loaded into the sample cell (i.e. between two coverslips). The suspension thus formed a monolayer colloidal glass. At high packing fraction, the sample was deeply jammed, but it still exhibited measureable thermal motion. Then the sample was heated and restabilized/equilibrated in a series of small temperature steps toward the jamming transition. At each step, 30 000 frames of bright-field video images were acquired and analyzed to derive the phonon modes. The Boson peak in the phonon density of states was very clearly observed in these jammed 2D colloidal glasses, and, more interestingly, the Boson peak was experimentally revealed to shift to lower frequencies and to increase in intensity as the packing fraction decreased towards the jamming transition (i.e. the solid–liquid fluidization point) as shown in figure 19. The trends observed were consistent with experimental observations of glasses under pressure and with predictions of jamming theory [156, 227, 261–263].

The excess modes near the Boson peak are often referred to as 'soft modes' because of their low energy. These modes are commonly observed in glasses, and their origin is still a matter of debate. The soft modes observed in the PNIPAM colloidal glasses could easily be visualized and were demonstrably quasi-localized with a participation ratio around 0.1 as shown in figure 16(*b*). Typically these modes involve tens to hundreds of neighboring particles. Theoretical studies have suggested that these soft modes, and in particular the soft spots associated with the large amplitude regions of the quasi-localized modes, are related to mechanical response of disordered solids. Specifically, it has been suggested that structural deformations or rearrangement regions tend to occur in regions at soft spots where soft mode amplitudes are large [156, 227, 261–263].

Chen *et al* studied the correlation between the soft modes and particle rearrangements in PNIPAM colloidal glasses, [264]. A quasi-2D colloidal glass similar to the ones studied in [67] was used, and the phonon modes were measured using displacement covariance analysis as before. But then the bulk compressive stress in the sample was changed, i.e. the sample temperature was increased slightly to reduce packing fraction and induce particle rearrangements. The rearranging particles were identified and were found to arise in clusters. These clusters, in turn, were found to be spatially correlated with soft modes and soft spots measured before the rearrangement events occurred, as shown in figure 20. This correlation suggests that regions where soft modes concentrate are more likely to experience deformations than other regions in the glassy colloid. This effect is somewhat similar to the behavior of regions with defects in crystalline solids [254, 265]. In fact, equivalent 'structural defects' or 'soft spots' can be defined for glasses using soft modes [262].

Glasses, in addition to being structurally disordered, can have disordered interparticle bond strengths. It is often difficult to separate the contributions of these two sources of disorder to the properties of glasses. Gratale *et al* studied

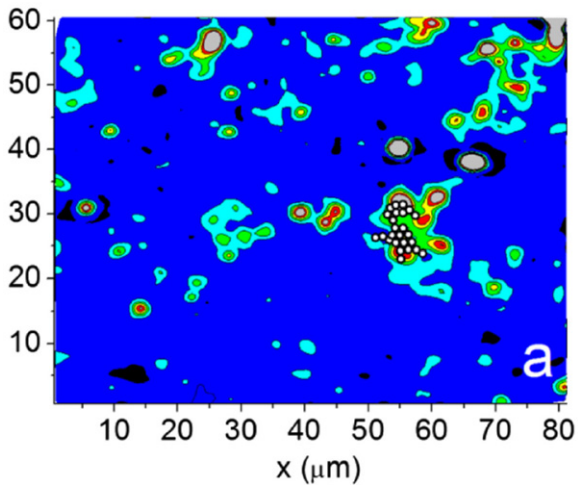

Figure 20. Color contour plots indicate polarization magnitudes for each particle, summed over the low-frequency modes, for 2D glass composed of PNIPAM particles. Regions that are red, green and gray represent soft spots in the colloidal glass. After the packing fraction is slightly decreased, some particles rearranged; circles indicate particles that rearranged. Rearranging particles typically are located on soft spots. (Figure reproduced with permission from [264] Copyright 2011 American Physical Society.)

the effects of bond-strength disorder on phonon modes in a crystalline lattice by applying displacement covariance matrix analysis to 2D crystals composed of PNIPAM and polystyrene (PS) particles [266]. Thus, these 2D crystalline samples consisted of soft PNIPAM particles doped randomly with similarly sized hard PS particles. This doping introduced three different interparticle bond strengths, namely soft–soft (PNIPAM–PNIPAM), soft–hard (PNIPAM–PS) and hard-hard (PS–PS). The experimenters found that phonon modes in colloidal crystals with bond-strength disorder follow Debye scaling at low frequencies, where the hard and soft particles participate equally. Medium-frequency modes are dominated by soft particle motion, while high-frequency modes mostly involve hard particle motions. Therefore, at least over the range of parameters studied, the bond-strength disorder did not lead to any obvious glassy properties such as the Boson peak.

Finally, very recently, the phonon mode methods have been extended to derive dispersion relations (i.e. phonon frequency versus wavevector curves) in colloidal crystals [254] and glasses [317]. The phonon curves enable determination of sound speeds, bulk moduli and shear moduli, which are proving potentially useful to elucidate possible effects of interparticle friction [317].

8. PNIPAM particles as depletants

It is well known that entropic effects produce a rich phase behavior in colloidal mixtures [12, 18, 268–282]. Entropically driven crystallization in binary particle suspensions, for example, can be induced at much lower particle volume fractions than their monodisperse counterparts. The concepts needed to understand mixtures of different size spherical particles were

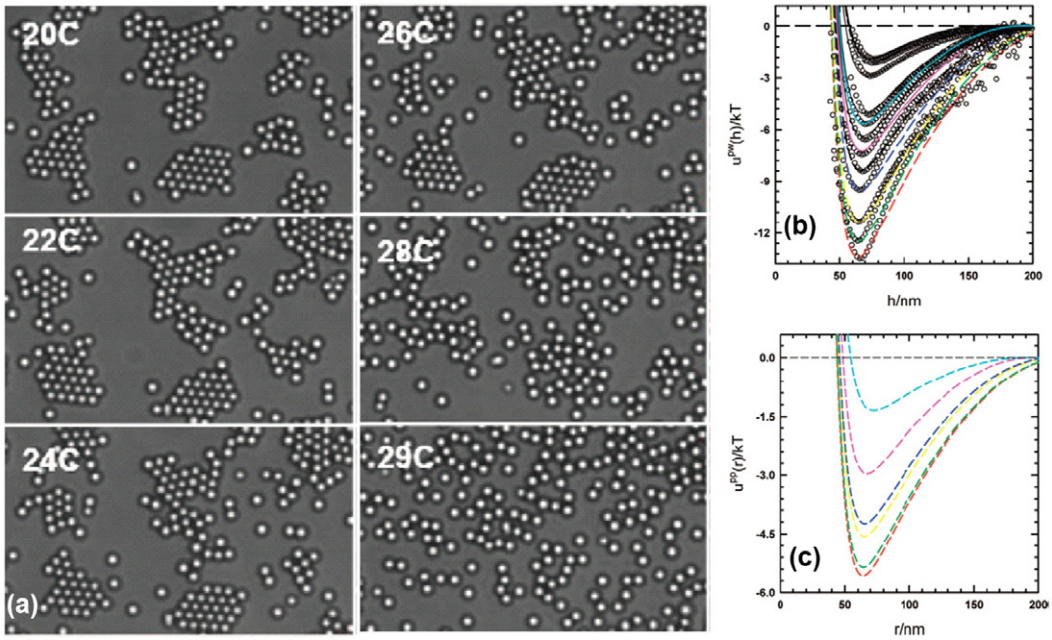

Figure 21. Quasi-2D colloidal configurations equilibriated at different temperatures for mixtures of 2.2 μm SiO_2 colloids and PNIPAM hydrogel depletants in 1.5 mM NaCl. (*b*) Particle–wall potential energy profiles obtained via Boltzmann inversion of the particle–wall separation probability distribution. (*c*) Particle–particle potential energy profiles obtained via inverse Monte Carlo analysis of experimental particle distributions. The figures are reproduced with permission from [267]. Copyright 2008 American Chemical Society.

first developed by Asakura and Oosawa [283, 284] and elaborated on by Vrij [285]. In such situations, an ordered arrangement of large spheres can increase the total suspension entropy by increasing the entropy of the small spheres. The essence of this entropic or so-called 'depletion' phenomena can be understood by considering the force between two large hard spheres with diameter a_L, induced by a sea of small hard spheres with diameter a_s. Because the center of mass of the small sphere cannot penetrate within a distance $a_s/2$ of the large sphere surface, a shell-like region of excluded volume surrounds each large sphere. Thus, when the surfaces of the two large spheres approach within a small-sphere diameter, these excluded volume regions overlap one another, and the total volume in the container accessible to the center of mass of the small spheres increases. The resulting increase in small sphere entropy induces an attractive *depletion* force between the large spheres. The attraction energy at contact scales according to $(a_L/a_s)\phi_s k_B T$, where ϕ_s is the small sphere volume fraction.

Notice that the strength of this interaction depends both on the volume fraction of the depletant particles, and the diameter ratio between the large particle and the depletant particle. In the vast majority of previous research on these problems, the strength of the depletion attraction is controlled by changing depletant concentration. With PNIPAM depletants, one can control the strength of depletion attraction between particles *in situ* with temperature or pH; of course, particle diameter changes are accompanied by volume fraction changes, so both effects must be considered.

Fernandes *et al* [267] were the first to utilize thermosensitive PNIPAM microspheres to create tunable depletion attraction. In their experiments, an aqueous solution containing ~2 μm diameter silica colloidal spheres and ~200 nm PNIPAM microgel spheres was placed in a 100 μl glass chamber (figure 21). The silica spheres settled into 2D colloidal packings at the bottom surface of the chamber due to their relatively high density and surface depletion forces [270, 288]. The experimenters utilized total internal reflection microscopy to measure particle–wall separation, and particle tracking by video microscopy to measure in-plane particle positions. As the temperature of this system was adjusted between 20 and 30 °C, the silica particles were found to reversibly form crystallites (low T) and then melt (high T).

Xing *et al* [289] later demonstrated that reversible depletion interactions of PNIPAM microspheres could also be manipulated via pH variation. In this work, Xing *et al* used a synthesis method to create PNIPAM-co-MAA microspheres that were resistant to temperature changes, but were very sensitive to changes in pH. The large-particle/wall interaction potential was derived from total internal reflection microscopy data as a function of microgel concentration and pH. For these particles, depletion attraction emerged at high pH (large PNIPAM diameter) and disappeared at low pH (small PNIPAM diameter).

With the possibility of using PNIPAM as a temperature- and/or pH-tunable depletant clearly demonstrated, several novel experiments then utilized the tunable entropic interaction as a facile means to explore and control self-assembly. Two experiments placed large particles into microwells and studied their behavior as a function of background PNIAPM depletant particles. Fernandes *et al* [290] etched shallow parabolic square 'wells' into a glass surface and filled the wells with silica particles at high concentration. These packings then

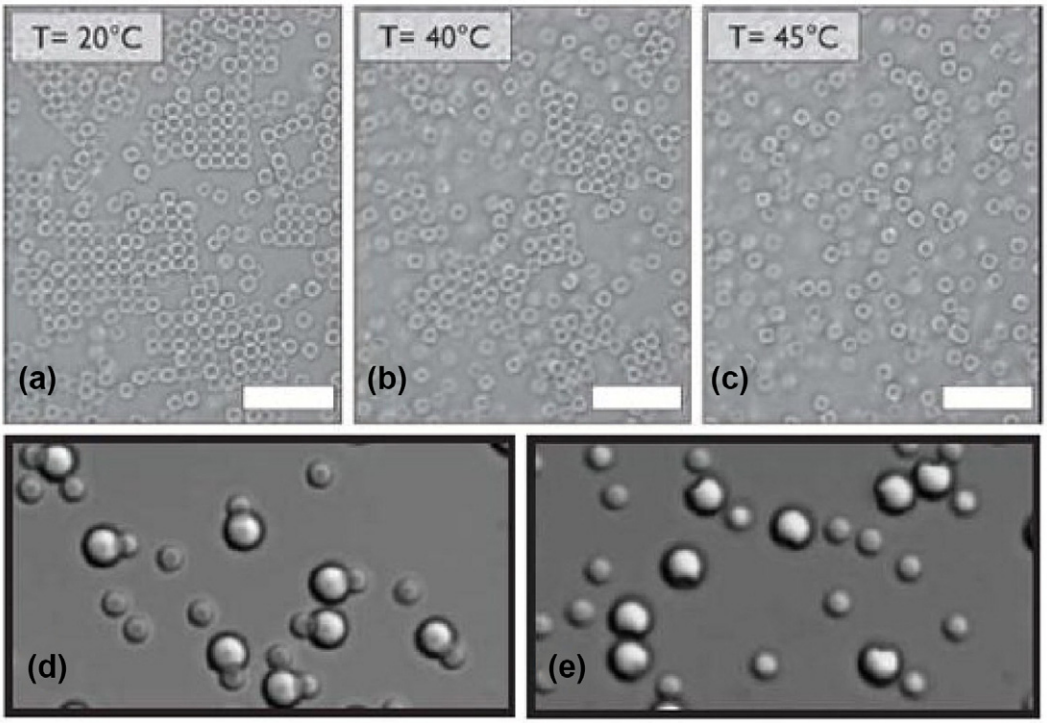

Figure 22. Temperature-dependent assembly of silica cuboids surrounded by ∼65 nm diameter PNIPAM hydrogel depletants. The scale bar is 20 μm. (Figure reproduced with permission from [286]. Copyright 2011 Royal Society of Chemistry.) (*d*)–(*e*) Selective assembly and disassembly of colloidal spheres and buckled shells at temperatures below (*d*) and above (*e*) the PNIPAM collapse temperature, respectively. Figures reproduced with permission from [287]. Copyright 2010 Nature Publishing Group.

reversibly transformed from quasi-2D fluids to crystallites with decreasing temperature. In a slightly different vein, Meng *et al* [291] used 80 nm PNIPAM particles as a depletant to affect small numbers of PS microspheres isolated in microwells; this configuration and approach enabled them to investigate the free energy landscape of 3D attractive hard-sphere clusters.

PNIPAM particle depletion has also been used as a mechanism for inducing novel self-assembly of non-spherical colloids. For example, Sacanna *et al* [287, 292] developed a method for synthesizing colloidal spheres with a concave spherical indentation. These concave particles were added to a depletant-filled solution with a number of slightly smaller colloidal spheres, i.e. slightly smaller spheres with potential to selectively 'fit' and 'lock' into the concavities of buckled particles with a similar radius of curvature (figures 22(*d*) and (*e*)). This colloidal lock-and-key concept relies on maximizing overlap of excluded free volume. The authors demonstrated this effect, and then they showed how tunable PNIPAM depletants can activate and de-activate this 'lock-and-key' pairing via temperature variation. Further, in a different publication the same group synthesized colloidal cuboids [286], placed them in a PNIPAM depletant solution, and tuned the interaction reversibly in order to assemble the cuboids into well-ordered cubic crystals (figures 22(*a*)–(*c*)) and sliding phases of cubes.

Interestingly, although the studies described above clearly demonstrate that PNIPAM microspheres are practical tools for inducing reversible colloidal self-assembly, recent work has shown that these particles do not always behave as ideal polymer depletants. Bayliss *et al*, for example, experimentally mapped out the differences in the phase diagram of a colloidal PS suspension depleted by PNIPAM microspheres against the phase diagram of a colloidal PS suspension depleted by a similar-size linear polymer coils [293]. Despite some similarities, the phase boundary of the arrested gel phase differed significantly between these two depletants. When compared with theoretical phase boundary predictions, it was found that PNIPAM microspheres behave more like hard spheres than the simpler model of non-interacting polymer depletant. Additionally, Zhao *et al* [271] showed that when PNIPAM particles adsorb to particle interfaces, arrested colloidal clusters are created not only via depletion, but also via 'bridging' particles which interact through non-specific binding mechanisms. Thus, when using PNIPAM particles as depletants, it is important to ensure that they do not adsorb to particle interfaces and that hard-sphere corrections to ideal depletion models are accounted for at high PNIPAM concentrations.

9. More effects in PNIPAM particle suspensions

Thus far this review concentrated on use of PNIPAM particles for study of the physics in colloidal solids and disordered packings. PNIPAM particles have also been used in a broad array of other investigations. Herein, we summarize some of this latter activity.

9.1. Optical properties

The thermoresponsive behavior of PNIPAM microgel particles can endow these complex fluids with interesting optical properties. Debord and Lyon found that at high packing fractions, PNIPAM crystals display bright iridescence in the visible region of the spectrum [294]. Then, as temperature is increased, the crystal melts and the sample becomes milky-white. This phase transition and accompanying optical response is reversible, permitting PNIPAM colloidal crystals to be manipulated in order to tune suspension color [295, 296].

As a result of these temperature-dependent optical responses, PNIPAM microgel particles have been explored as a means to create new optical devices and photonic materials [56, 297, 298]. For example, by placing a thin layer of PNIPAM particle suspension between two reflective surfaces, a device similar to a Fabry–Pérot etalon is created. The reflection spectrum of this type of device can be altered by changing the temperature or pH [297]. In a related vein, self-assembled colloidal crystals of PNIPAM microgel particles appear nearly transparent at low temperatures, since swollen PNIPAM have nearly the same index of refraction as water, but the crystals Bragg diffract visible, infrared and ultraviolet light at temperatures above the deswelling temperature [56]. Such PNIPAM colloidal crystals can be polymerized into an acrylamide/bisacrylamide hydrogel, which constrains hydrogel particle center-of-mass position while maintaining their volume-changing temperature dependence. A fast temperature jump from 30 to 35 °C causes the hydrogel to switch from diffracting very little light to diffracting almost all light on timescales of order 1 ms or less [298].

9.2. PNIPAM suspensions in electric fields

In a different vein, charged PNIPAM particle suspensions at varying effective packing fractions, ζ (as defined above [210]), have been demonstrated to exhibit novel structures in the presence of external electric fields [299]. At low packing fractions ($\zeta = 0.1$), well below the glass transition, strings of PNIPAM particles assembled, creating a fluid of strings. At higher packing fractions, $\zeta = 0.85$, above the glass transition, the suspensions exhibited a re-entrant disorder–order–disorder transition; with zero applied electric field, the dense packings were amorphous, and when the field was turned on to sufficient strength, the packings crystallized. Upon increasing the field strength further, a phase-separated state consisting of a solid phase and a disordered gas phase was observed. Thus, the combination of external fields and particle swelling and deswelling yields media that are phenomenologically rich and worthy of further investigation.

9.3. PNIPAM particle softness effects

The softness of PNIPAM microgel particles appear to have precipitated some interesting (if not as yet fully understood) effects in their own right. In one study [301], a PNIPAM colloidal crystal was doped with larger PNIPAM particles whose diameter was more than twice the diameter of the majority PNIPAM particles. Surprisingly, it was observed

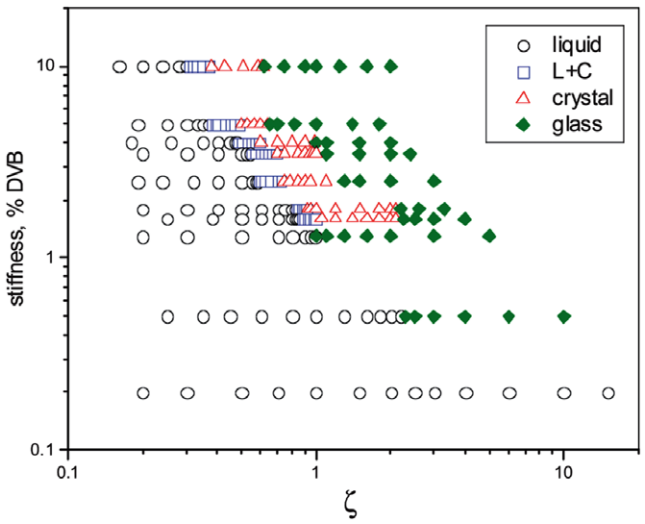

Figure 23. Phase diagram of microgels as a function of stiffness. Stiffness is given as percentage of crosslinker divinylbenzene (DVB) used in microgel synthesis. Generalized volume fraction $\zeta = nV$, with n the number of microgels and V the volume of the microgel measured at low concentration is given as x-axis. Figure reproduced with permission from [300]. Copyright 2012 Royal Society of Chemistry.

that the larger dopant particles would generally shrink to fit properly into the crystalline lattice. Careful study of particle trajectories showed that these larger particles were not forced into a location on the lattice, but that they simply deswelled to fit into the lattice.

Sierra-Martin and Fernandez-Nieves have also carried out rheology, and UV–visible spectroscopy studies that indicate that particle softness can qualitatively affect the phase behavior of microgel suspensions [300]. Suspensions of relatively stiff particles were found to transition from liquid to crystal to glass as the volume fraction increased, i.e. they produced the same three phases found in hard-sphere suspensions (figure 23). By contrast, suspensions composed of particles of intermediate stiffness were found to transition from liquid to glass as the volume fraction increased, with the crystal phase disappearing. Lastly, suspensions of the softest particles were only found in the liquid state, no crystal or glass state was observed at the volume fractions studied.

9.4. PNIPAM suspensions: pH effects

As noted earlier, the properties of PNIPAM microgels can be manipulated using pH. Cho *et al* studied the interactions between microgel particles as a function of pH [53]. They found that at low pH (pH < 6) PNIPAM particles which incorporated acrylic acid groups were weakly attractive, but at high pH, these particles were purely repulsive (figure 24). The authors attributed the weak attraction at low pH to hydrogen bonding, and the repulsion at high pH to electrostatic interactions. Muluneh *et al* used this pH sensitivity to study the 3D structural and dynamical evolution of PNIPAM microgel particle suspensions after a quench from the liquid state [302]. At low pH and volume fraction, crystallization due

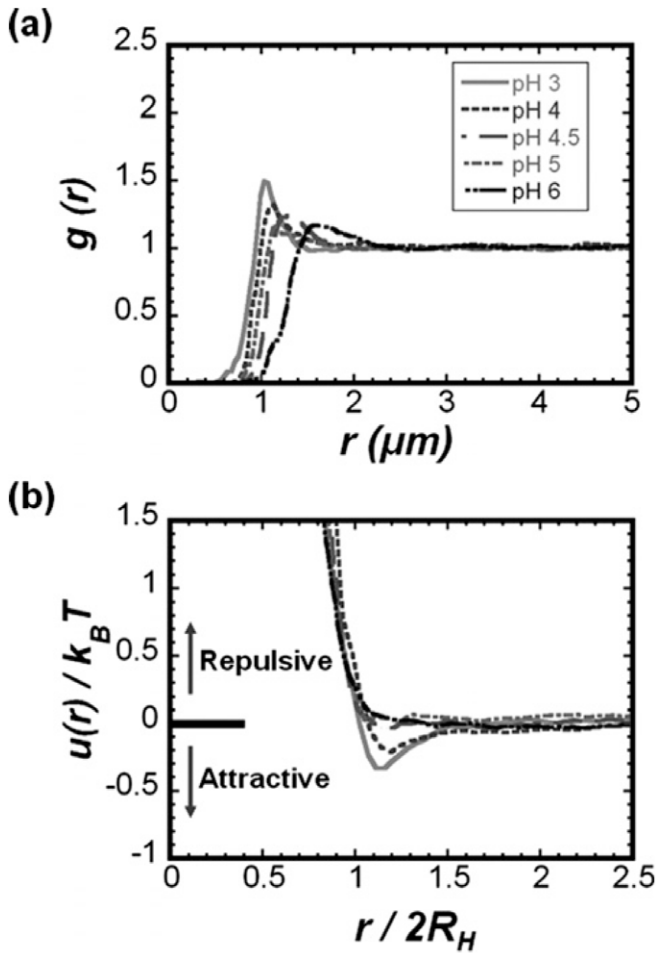

Figure 24. (*a*) Pair-correlation function $g(r)$ as a function of separation distance r for suspensions of PNIPAM-*co*-AAc core–shell particles at different pH. (*b*) Interaction potential between core–shell particles at different pH as a function of normalized separation distance. R_H is the hydrodynamic radius of the core–shell particles found using Stokes–Einstein relation of the measured MSD. Figure reproduced with permission from [53]. Copyright 2009 Royal Society of Chemistry.

to the attraction between particles was suggested as the main cause for dynamical arrest. At low pH and high volume fraction, relaxation was constrained and a disordered solid formed. At neutral pH, wherein particles are purely repulsive, a disordered soft glassy solid was formed at high volume fraction. Finally, Meng *et al* studied aging of suspensions of PNIPAM particles with incorporated acrylic acid groups and found that aging behavior is quite different as a function of pH [81]. Specifically, at low pH the suspensions were observed to evolve (via aging) into a crystal at surprisingly low volume fractions (40%), but at high pH the suspensions remained fluid even at extremely high volume fractions.

9.5. Thermoresponsive colloidal gels

When PNIPAM microgel particles are immersed in an aqueous suspension with a sufficient ion concentration, heating above the LCST produces a strong, short-ranged interparticle attraction due to a combination of van der Waals forces and hydrophobic effects. At sufficiently high concentrations, this effect creates a reversible colloidal gel [303–305]. A particularly interesting potential application of this material is for injectable colloidal gel scaffolds; such room-temperature colloidal fluids can be non-invasively injected into patients; once inside the body, they form rigid gels upon heating to body temperature wherein they act as scaffolds for new cell growth [305–307], or as depots for controlled drug release [304]. Though other thermo-sensitive polymers have been considered for similar applications, colloidal PNIPAM gels have comparative benefits of low initial viscosity, improved mechanical properties, and the ability to load gradual-releasing agents to guide cell growth [304–307]. Thermoresponsive PNIPAM microgels may also have applications as switchable cell culture substrates [112].

The bulk of the studies of this system class, however, have focused on chemical modification of PNIPAM particles and surrounding fluid to modify various bulk gel properties, including thermal reversibility [308], biodegradability [309] and susceptibility to syneresis, i.e. the displacement of fluid from a gel [306, 307]. Additionally, PNIPAM colloidal gels have been created by depletion-driven aggregation using non-adsorbing polymer and subsequent crosslinking [310, 311]. Recent rheological studies have investigated the interplay of inter-particle interaction modifications, via salt and temperature modification, on the bulk gel kinetics [312] and structure [313]. Ultimately, these types of studies could be expanded to explore the physics and phase behavior of attractive particle packings, but such work will require improved quantification of the temperature- and salt-dependencies of the short-range particle interaction potentials.

10. Future

Many more interesting experiments are possible with PNIPAM particles. The use of local perturbations such as optical heating, for example, offers interesting possibilities with respect to superheating [170] and super-cooling and subsequent sample evolution, as well as for microscopic studies of mechanical response. The role played by particle stiffness in affecting the mechanical properties of glasses has begun to be investigated, e.g. [210], but many interesting questions remain in this context and even less work has been done to probe the role of particle stiffness on the mechanical properties of ordered systems. Along another direction, recent work exploring phonons in disordered systems should stimulate more experiments, particularly about the connection of mechanical instabilities to phonons, as well as about the detailed nature of the density of states in ordered versus partially ordered systems.

Finally, while this review has focused on the behavior of PNIPAM particles in bulk fluids, recent experiments have also shown that PNIPAM particles exhibit intriguing properties on interfaces (e.g. the air–water interface) [314, 315]. PNIPAM particles, for example, were found to be especially good stabilizers for Pickering emulsions [314, 318]. This effect is apparently due to the fact that PNIPAM particles flatten upon adsorption [314, 315]. Thus, novel solid-like phases composed of PNIPAM particles likely form on air–water and oil–water interfaces; they will be interesting objects for future study.

Acknowledgments

For useful insights and experimental advice about PNIPAM early on, we gratefully thank our colleagues Ahmed Alsayed, Yilong Han and Zexin Zhang. For discussions about research presented in this review, and more, we also thank Kevin Aptowicz, Anindita Basu, Daniel Chen, Zoey Davidson, Doug Durian, Wouter Ellenbroek, Carl Goodrich, Piotr Habdas, Randy Kamien, Andrea Liu, Tom Lubensky, Tony Maggs, Lisa Manning, Kerstin Nordstrom, Michael Schindler, Yair Shokef, Eric Weeks, Qi Wen and Ye Xu. We also gratefully acknowledge financial support from the National Science Foundation through Grants DMR11-20901 (MRSEC) and DMR12-05463, and support from NASA Grant NNX08AO0G. T S acknowledges financial support from DAAD.

References

[1] Hunter R J 2001 *Foundations of Colloid Science* 2nd edn (Oxford: Oxford University Press)
[2] Poon W C K, Weeks E R and Royall C P 2012 *Soft Matter* **8** 21
[3] Weeks E, Crocker J C, Levitt A C, Schofield A and Weitz D 2000 *Science* **5453** 627–31
[4] Pusey P N and van Megen W 1986 *Nature* **320** 340
[5] Brambilla G, Masri D E, Pierno M, Berthier L, Cipelletti L, Petekidis G and Schofield A B 2009 *Phys. Rev. Lett.* **102** 085703
[6] Anderson V J and Lekkerkerker H N W 2002 *Nature* **416** 811
[7] Dhont J K G, Smits C and Lekkerkerker H N W 1992 *J. Colloid Interface Sci.* **152** 386
[8] Dinsmore A D, Yodh A G and Pine D J 1995 *Phys. Rev.* E **52** 4045
[9] Sirota E B, Yang H D O, Sinha S K, Chaikin P M, Axe J D and Fujii Y 1989 *Phys. Rev. Lett.* **62** 1524
[10] Monovoukas Y and Gast A P 1989 *J. Colloid Interface Sci.* **128** 533
[11] Pham K N, Puertas A M, Bergenholtz J, Egelhaaf S U, Moussaïd A, Pusey P N, Schofield A B, Cates M E, Fuchs M and Poon W C K 2002 *Science* **296** 104
[12] Ilett S M, Orrock A, Poon W C K and Pusey P N 1995 *Phys. Rev.* E **51** 1344
[13] Marcus A H and Rice S A 1996 *Phys. Rev. Lett.* **77** 2577
[14] Mason T G, Bibette J and Weitz D A 1995 *Phys. Rev. Lett.* **75** 2051
[15] Mason T G, Lacasse M D, Grest G S, Levine D, Bibette J and Weitz D A 1997 *Phys. Rev.* E **56** 3150
[16] Royall C P, Vermolen E C M, van Blaaderen A and Tanaka H 2008 *J. Phys.: Condens. Matter* **20** 404225
[17] Pieranski P, Strzelecki L and Pansu B 1983 *Phys. Rev. Lett.* **50** 900
[18] Latka A, Han Y, Alsayed A M, Schofield A B, Yodh A G and Habdas P 2009 *Europhys. Lett.* **86** 58001
[19] Trappe V, Prasad V, Cipelletti L, Segre P N and Weitz D A 2001 *Nature* **411** 772
[20] Zhang Z, Yunker P J, Habdas P and Yodh A G 2011 *Phys. Rev. Lett.* **107** 208303
[21] Yunker P J, Chen K, Zhang Z and Yodh A G 2011 *Phys. Rev. Lett.* **106** 225503
[22] Lu P J, Conrad J C, Wyss H M, Schofield A B and Weitz D A 2006 *Phys. Rev. Lett.* **96** 028306
[23] Zahn K, Lenke R and Maret G 1999 *Phys. Rev. Lett.* **82** 2721
[24] Senff H and Richtering W 1999 *J. Chem. Phys.* **111** 1705
[25] Pelton R 2000 *Adv. Colloid Interface Sci.* **85** 1
[26] Wu C, Zhou S, Au-yeung S C F and Jiang S 1996 *Die Angew. Makromol. Chem.* **240** 123
[27] Lele A K, Hirve M M, Badiger M V and Mashelkar R A 1997 *Macromolecules* **30** 157
[28] Takeuchi S, Oike M, Kowitz C, Shimasaki C, Hasegawa K and Kitano H 1993 *Die Makromol. Chem.* **194** 551
[29] Serizawa T, Chen M-Q and Akashi M 1998 *J. Polym. Sci.* **36** 2581
[30] Duracher D, Elaïssari A, and Pichot C 1999 *Colloid Polym. Sci.* **277** 905
[31] Duracher D, Elaïssari A and Pichot C 1999 *J. Polym. Sci.* A **37** 1823
[32] Richtering W (ed) 2006 *Smart Colloidal Materials* (*Progress in Colloid and Polymer Science* vol 133) (Berlin: Springer) ISBN 9783540327011
[33] Fernandez-Nieves A, Wyss H, Mattsson J and Weitz D 2011 *Microgel Suspensions: Fundamentals and Applications* (New York: Wiley) ISBN 9783527633012
[34] Jochum F D, Roth P J, Kessler D and Theato P 2010 *Biomacromolecules* **11** 2432
[35] Plamper F A, Steinschulte A A, Hofmann C H, Drude N, Mergel O, Herbert C, Erberich M, Schulte B, Winter R and Richtering W 2012 *Macromolecules* **45** 8021
[36] Ahn S-k, Kasi R M, Kim S-C, Sharma N and Zhou Y 2008 *Soft Matter* **4** 1151
[37] Wong J E and Richtering W 2008 *Curr. Opin. Colloid Interface Sci.* **13** 403
[38] Pich A, Richtering W and Albrecht K 2010 *Chemical Design of Responsive Microgels* (*Advances in Polymer Science*) (Berlin: Springer) ISBN 9783642163784
[39] Lyon L A and Nieves A F 2012 *Annu. Rev. Phys. Chem.* **63** 25
[40] Pelton R 2010 *J. Colloid Interface Sci.* **348** 673
[41] Bae Y H, Okano T and Kim S W 1990 *J. Polym. Sci.* B **28** 923
[42] Wongsuwarn S, Vigolo D, Cerbino R, Howe A M, Vailati A, Piazza R and Cicuta P 2012 *Soft Matter* **8** 5857
[43] Koniger A, Plack N, Kohler W, Siebenburger M and Ballauff M 2013 *Soft Matter* **9** 1418
[44] Ruckenstein E 1981 *J. Colloid Interface Sci.* **83** 77 www.sciencedirect.com/science/article/pii/0021979781900114
[45] Duhr S and Braun D 2006a *Phys. Rev. Lett.* **96** 168301
[46] Duhr S and Braun D 2006b *Proc. Natl Acad. Sci.* **103** 19678 www.pnas.org/content/103/52/19678.full.pdf+html, URL www.pnas.org/content/103/52/19678.abstract
[47] Braibanti M, Vigolo D and Piazza R 2008 *Phys. Rev. Lett.* **100** 108303
[48] Saunders B R and Vincent B 1999 *Adv. Colloid Interface Sci.* **80** 1
[49] Han Y, Ha N Y, Alsayed A M and Yodh A G 2008a *Phys. Rev.* E **77** 041406
[50] Han Y, Shokef Y, Alsayed A M, Yunker P, Lubensky T C and Yodh A G 2008 *Nature* **456** 898
[51] Baumgartl J and Bechinger C 2005 *Europhys. Lett.* **71** 487
[52] Alsayed A M, Han Y and Yodh A 2011 Melting and geometric frustration in temperature-sensitive colloids *Microgel Suspensions* (Weinheim: Wiley-VCH) pp 229–81
[53] Cho J K, Meng Z, Lyon L A and Breedveld V 2009 *Soft Matter* **5** 3599
[54] Wolfe M and Scopazzi C 1989 *J. Colloid Interface Sci.* **133** 265
[55] Kratz K, Hellweg T and Eimer W 2000 *Colloids Surf.* A **170** 137
[56] Weissman J M Sunkara H B, Tse A S and Asher S A 1996 *Science* **274** 959
[57] Zhou S and Chu B 1998 *J. Phys. Chem.* B **102** 1364
[58] Senff H and Richtering W 2000 *Colloid Polym. Sci.* **278** 830
[59] Jones C D and Lyon L A 2003 *Macromolecules* **36** 1988
[60] Hoare T and Pelton R 2007 *Macromolecules* **40** 670

[61] Garcia A, Marquez M, Cai T, Rosario R, Hu Z, Gust D, Hayes M, Vail S A and Park C-D 2006 *Langmuir* **23** 224
[62] Stieger M, Pedersen J S, Lindner P and Richtering W 2004 *Langmuir* **20** 7283
[63] Wang J, Gan D, Lyon L A and El-Sayed M A 2001 *J. Am. Chem. Soc.* **123** 11284
[64] Wu J, Zhou B and Hu Z 2003 *Phys. Rev. Lett.* **90** 048304
[65] Wu C and Zhou S 1996 *J. Polym. Sci.* B **34** 1597
[66] Debord S B and Lyon L A 2003 *J. Phys. Chem.* B **107** 2927
[67] Chen K *et al* 2010 *Phys. Rev. Lett.* **105** 025501
[68] Nordstrom K N, Verneuil E, Ellenbroek W G, Lubensky T C, Gollub J P and Durian D J 2010 *Phys. Rev.* E **82** 041403
[69] Pelton R H, Pelton H M, Morphesis A and Rowell R L 1989 *Langmuir* **5** 816
[70] Yao Z L, Grishkewich N and Tam K C 2013 *Soft Matter* **9** 5319–35
[71] Zhang J-T, Liu X-L, Fahr A and Jandt K 2008 *Colloid Polym. Sci.* **286** 1209
[72] Murray M,Charlesworth D, Swires L, Riby P, Cook J, Chowdhry B Z and Snowden M J 1994 *J. Chem. Soc. Faraday Trans.* **90** 1999
[73] Wu X, Pelton R H, Hamielec A E, Woods D R and McPhee W 1994 *Colloid Polym. Sci.* **272** 467
[74] Stieger M, Richtering W, Pedersen J S and Lindner P 2004 *J. Chem. Phys.* **120** 6197
[75] Meyer S and Richtering W 2005 *Macromolecules* **38** 1517
[76] Reufer M, Diaz-Leyva P and Scheffold F 2009 *Eur. Phys. J.* E **28** 165
[77] Mason T G and Lin M Y 2005 *Phys. Rev.* E **71** 040801
[78] Acciaro R, Gilányi T and Varga I 2011 *Langmuir* **27** 7917
[79] Still T, Chen K, Alsayed A M, Aptowicz K B and Yodh A G 2013 *J. Colloid Interface Sci.* **405** 96
[80] Shimizu H, Wada R and Okabe M 2009 *Polym. J* **41** 771
[81] Meng Z, Cho J K, Breedveld V and Lyon L A 2009 *J. Phys. Chem.* B **113** 4590
[82] Meunier F, Elaissari A and Pichot C 1995 *Polym. Adv. Technol.* **6** 489
[83] Alsayed A M, Islam M F, Zhang J, Collings P J and Yodh A G 2005 *Science* **309** 1207
[84] Chu L-Y, Kim J-W, Shah R and Weitz D 2007 *Adv. Funct. Mater.* **17** 3499
[85] Kim J-W, Utada A, Fernández-Nieves A, Hu Z and Weitz D 2007 *Angew. Chem. Int. Edn* **46** 1819
[86] Park T G and Hoffman A S 1992 *J. Polym. Sci.* A **30** 505
[87] Karg M, Pastoriza-Santos I, Liz-Marzán L M and Hellweg T 2006 *ChemPhysChem* **7** 2298
[88] Karg M, Wellert S, Prevost S, Schweins R, Dewhurst C, Liz-Marzán L and Hellweg T 2011 *Colloid Polym. Sci.* **289** 699
[89] Dingenouts N, Norhausen C and Ballauff M 1998 *Macromolecules* **31** 8912
[90] Boyer C, Whittaker M R Luzon M and Davis T P 2009 *Macromolecules* **42** 6917
[91] Deng Y, Yang W, Wang C and Fu S 2003 *Adv. Mater.* **15** 1729
[92] Rahman M M, Chehimi M M, Fessi H and Elaissari A 2011 *J. Colloid Interface Sci.* **360** 556
[93] Kraft D J, Hilhorst J, Heinen M A P, Hoogenraad M J, Luigjes B and Kegel W K 2011 *J. Phys. Chem.* B **115** 7175
[94] Pelton R and Chibante P 1986 *Colloids Surf.* **20** 247
[95] Crassous J J, Ballauff M, Drechsler M, Schmidt J and Talmon Y 2006 *Langmuir* **22** 2403
[96] Crassous J J, Rochette C N, Wittemann A, Schrinner M, Ballauff M and Drechsler M 2009 *Langmuir* **25** 7862
[97] Okay O 2009 General properties of hydrogels *Hydrogel Sensors and Actuators* (*Springer Series on Chemical Sensors and Biosensors* vol 6) (Berlin: Springer) pp 1–15
[98] Garcia-Salinas M J and Donald A M 2010 *J. Colloid Interface Sci.* **342** 629
[99] St John A N, Breedveld V and Lyon L A 2007 *J. Phys. Chem.* B **111** 7796
[100] Carpenter D K 1977 *J. Chem. Educ.* **54** A430
[101] Johnson C S and Gabriel D A 1995 *Laser Light Scattering* corrected edn (*Dover Books on Physics*) (New York: Dover) ISBN 0486683281
[102] Deen G R, Alsted T, Richtering W and Pedersen J S 2011 *Phys. Chem. Chem. Phys.* **13** 3108
[103] McPhee W, Tam K C and Pelton R 1993 *J. Colloid Interface Sci.* **156** 24
[104] Mie G 1908 *Ann. Phys.* **330** 377
[105] Berne B J and Pecora R 2000 *Dynamic Light Scattering* (Mineola: Dover)
[106] Wu C and Wang X 1998 *Phys. Rev. Lett.* **80** 4092
[107] Gasser U, Lietor-Santos J-J, Scotti A, Bunk O, Menzel A and Fernandez-Nieves A 2013 *Phys. Rev.* E **88** 052308
[108] Crowther H M, Saunders B R, Mears S J, Cosgrove T, Vincent B, King S M and Yu G-E 1999 *Colloids Surf.* A **152** 327
[109] Fernández-Barbero A, Fernández-Nieves A, Grillo I and López-Cabarcos E 2002 *Phys. Rev.* E **66** 051803
[110] Pedersen J S 1997 *Adv. Colloid Interface Sci.* **70** 171
[111] Hoare T and McLean D 2006 *J. Phys. Chem.* B **110** 20327
[112] Schmidt S, Zeiser M, Hellweg T, Duschl C, Fery A and Möhwald H 2010 *Adv. Funct. Mater.* **20** 3235
[113] Lowe J S, Chowdhry B Z, Parsonage J R and Snowden M J 1998 *Polymer* **39** 1207
[114] Kiminta D O, Luckham P and Lenon S 1995 *Polymer* **36** 4827
[115] Mielke M and Zimehl R 1998 *Ber. Bunsenges. Phys. Chem.* **102** 1698
[116] Senff H, Richtering W, Norhausen C, Weiss A and Ballauff M 1999 *Langmuir* **15** 102
[117] Carrier V and Petekidis G 2009 *J. Rheol.* **53** 245
[118] Brugger B, Vermant J and Richtering W 2010 *Phys. Chem. Chem. Phys.* **12** 14573
[119] Crassous J J, Siebenburger M, Ballauff M, Drechsler M, Henrich O and Fuchs M 2006 *J. Chem. Phys.* **125** 204906
[120] Siebenburger M, Fuchs M and Ballauff M 2012 *Soft Matter* **8** 4014
[121] Hashmi S M and Dufresne E R 2009 *Soft Matter* **5** 3682
[122] Liu A J and Nagel S R 1998 *Nature* **396** 21
[123] O'Hern C S, Silbert L E, Liu A J and Nagel S R 2003 *Phys. Rev.* E **68** 011306
[124] Silbert L E, Liu A J and Nagel S R 2006 *Phys. Rev.* E **73** 041304
[125] Silbert L E, Liu A J and Nagel S R 2005 *Phys. Rev. Lett.* **95** 098301
[126] Tighe B P 2011 *Phys. Rev. Lett.* **107** 158303
[127] Tighe B P, Woldhuis E, Remmers J J C, van Saarloos W and van Hecke M 2010 *Phys. Rev. Lett.* **105** 088303
[128] Vitelli V, Xu N, Wyart M, Liu A J and Nagel S R 2010 *Phys. Rev.* E **81** 021301
[129] Wang L and Xu N 2013 *Soft Matter* **9** 2475
[130] Xu N, Vitelli V, Wyart M, Liu A J and Nagel S R 2009 *Phys. Rev. Lett.* **102** 038001
[131] Zeravcic Z, Xu N, Liu A J, Nagel S R and Saarloos W V 2009 *Europhy. Lett.* **87** 26001
[132] Zhang Z, Xu N, Chen D T N, Yunker P, Alsayed A M, Aptowicz K B, Habdas P, Liu A J, Nagel S R and Yodh A G 2009 *Nature* **459** 230
[133] Nordstrom K N, Verneuil E, Arratia P E, Basu A, Zhang Z, Yodh A G, Gollub J P and Durian D J 2010 *Phys. Rev. Lett.* **105** 175701
[134] Corwin E I, Jaeger H M and Nagel S R 2005 *Nature* **435** 1075
[135] Xu N, Wyart M, Liu A J and Nagel S R 2007 *Phys. Rev. Lett.* **98** 175502
[136] Wyart M 2010 *Europhys. Lett.* **89** 64001

[137] Basu A, Xu Y, Still T, Arratia P E, Zhang Z, Nordstrom K N, Rieser J M, Gollub J P, Durian D J and Yodh A G 2014 *Soft Matter* **10** 3027

[138] Berthier L, Jacquin H and Zamponi F 2011 *Phys. Rev.* E **84** 051103

[139] Brito C, Dauchot O, Biroli G and Bouchaud J-P 2010 *Soft Matter* **6** 3013

[140] Candelier R and Dauchot O 2010 *Phys. Rev.* E **81** 011304

[141] Charbonneau P, Corwin E I, Parisi G and Zamponi F 2012 *Phys. Rev. Lett.* **109** 205501

[142] Chaudhuri P, Berthier L and Kob W 2007 *Phys. Rev. Lett.* **99** 060604

[143] Cheng X 2010 *Phys. Rev.* E **81** 031301

[144] Coulais C, Behringer R P and Dauchot O 2012 *Europhy. Lett.* **100** 44005

[145] Dauchot O, Marty G and Biroli G 2005 *Phys. Rev. Lett.* **95** 265701

[146] Dijksman J A, Wortel G H, van Dellen L T H, Dauchot O and van Hecke M 2011 *Phys. Rev. Lett.* **107** 108303

[147] Donev A, Cisse I, Sachs D, Variano E A, Stillinger F H, Connelly R, Torquato S and Chaikin P M 2004 *Science* **303** 990

[148] Ellenbroek W G, van Hecke M and van Saarloos W 2009 *Phys. Rev.* E **80** 061307

[149] Ellenbroek W G, Somfai E, van Hecke M and van Saarloos W 2006 *Phys. Rev. Lett.* **97** 258001

[150] Ellenbroek W G, Zeravcic Z, van Saarloos W and van Hecke M 2009 *Europhys. Lett.* **87** 34004

[151] Gómez L R, Turner A M, van Hecke M and Vitelli V 2012 *Phys. Rev. Lett.* **108** 058001

[152] Goodrich C P, Liu A J and Nagel S R 2012 *Phys. Rev. Lett.* **109** 095704

[153] Henkes S, van Hecke M and van Saarloos W 2010 *Europhys. Lett.* **90** 14003

[154] Ikeda A, Berthier L and Sollich P 2013 *Soft Matter* **9** 7669–83

[155] Ikeda A, Berthier L and Sollich P 2012 *Phys. Rev. Lett.* **109** 018301

[156] Wyart M, Nagel S R and Witten T A 2005 *Europhys. Lett.* **72** 486

[157] Mailman M, Schreck C F, O'Hern C S and Chakraborty B 2009 *Phys. Rev. Lett.* **102** 255501

[158] Olsson P and Teitel S 2011 *Phys. Rev.* E **83** 030302

[159] Olsson P and Teitel S 2007 *Phys. Rev. Lett.* **99** 178001

[160] Olsson P and Teitel S 2012 *Phys. Rev. Lett.* **109** 108001

[161] Brader J M, Voigtmann T, Fuchs M, Larson R G and Cates M E 2009 *Proc. Natl Acad. Sci.* **106** 15186

[162] Brader J M, Cates M E and Fuchs M 2008 *Phys. Rev. Lett.* **101** 138301

[163] Ikeda A, Berthier L and Biroli G 2013 *J. Chem. Phys.* **138** 12A507

[164] Voudouris P, Florea D, van der Schoot P and Wyss H M 2013 *Soft Matter* **9** 7158–66

[165] Scheffold F, Diaz-Leyva P, Reufer M, Ben Braham N, Lynch I and Harden J L 2010 *Phys. Rev. Lett.* **104** 128304

[166] Romeo G and Ciamarra M P 2013 *Soft Matter* **9** 5401

[167] Sierra-Martín B, Laporte Y, South A B, Lyon L A and Fernández-Nieves A 2011 *Phys. Rev.* E **84** 011406

[168] Nguyen V D, Hu Z and Schall P 2011 *Phys. Rev.* E **84** 011607

[169] Gokhale S, Nagamanasa K H, Santhosh V, Sood A K and Ganapathy R 2012 *Proc. Natl Acad. Sci.* **109** 20314

[170] Wang Z, Wang F, Peng Y, Zheng Z and Han Y 2012 *Science* **338** 87

[171] Daeges J, Gleiter H and Perepezko J 1986 *Phys. Lett.* A **119** 79

[172] Herman J W and Elsayed-Ali H E 1992 *Phys. Rev. Lett.* **69** 1228

[173] Banhart F, Hernandez E and Terrones M 2003 *Phys. Rev. Lett.* **90** 185502

[174] Siwick B J, Dwyer J R, Jordan R E and Miller R D 2003 *Science* **302** 1382

[175] Kosterlitz J M and Thouless D J 1973 *J. Phys. C: Solid State Phys.* **6** 1181

[176] Nelson D R and Halperin B I 1979 *Phys. Rev.* B **19** 2457

[177] Young A P 1979 *Phys. Rev.* B **19** 1855

[178] Nelson D 2002 *Defects and Geometry in Condensed Matter Physics* (Cambridge: Cambridge University Press)

[179] Zahn K and Maret G 2000 *Phys. Rev. Lett.* **85** 3656

[180] Murray C A and Van Winkle D H 1987 *Phys. Rev. Lett.* **58** 1200

[181] von Grünberg H H, Keim P, Zahn K and Maret G 2004 *Phys. Rev. Lett.* **93** 255703

[182] Peng Y, Wang Z, Alsayed A M, Yodh A G and Han Y 2010 *Phys. Rev. Lett.* **104** 205703

[183] Moessner R and Ramirez A P 2006 *Phys. Today* **59** 24

[184] Harris M J, Bramwell S T, McMorrow D F, Zeiske T and Godfrey K W 1997 *Phys. Rev. Lett.* **79** 2554

[185] Ramirez A 2003 *Nature* **421** 483

[186] Wang R *et al* 2006 *Nature* **439** 303

[187] Wannier G 1973 *Phys. Rev.* B **7** 5017

[188] Shokef Y, Souslov A and Lubensky T C 2011 *Proc. Natl Acad. Sci.* **108** 11804

[189] Shokef Y and Lubensky T C 2009 *Phys. Rev. Lett.* **102** 048303

[190] Weiss J A, Oxtoby D W, Grier D G and Murray C A 1995 *J. Chem. Phys.* **103** 1180

[191] Pansu B, Pieranski P and Pieranski P 1984 *J. Phys.* **45** 331

[192] Osterman N, Babič D, Poberaj I, Dobnikar J and Ziherl P 2007 *Phys. Rev. Lett.* **99** 248301

[193] Shokef Y, Han Y, Souslov A, Yodh A G and Lubensky T C 2013 *Soft Matter* **9** 6565

[194] Nisoli C, Wang R, Li J, McConville W F, Lammert P E, Schiffer P and Crespi V H 2007 *Phys. Rev. Lett.* **98** 217203

[195] Davidović D, Kumar S, Reich D H, Siegel J, Field S B, Tiberio R C, Hey R and Ploog K 1996 *Phys. Rev. Lett.* **76** 815

[196] Hilgenkamp H, Ariando, Smilde H-J H, Blank D H A, Rijnders G, Rogalla H, Kirtley J R and Tsuei C C 2003 *Nature* **422** 50

[197] Libál A, Reichhardt C and Reichhardt C J O 2006 *Phys. Rev. Lett.* **97** 228302

[198] Watanabe K and Tanaka H 2008 *Phys. Rev. Lett* **100** 158002

[199] Abate A R and Durian D J 2008 *Phys. Rev. Lett.* **101** 245701

[200] Sheng H W, Luo W K, Alamgir F M, Bai J M and Ma E 2007 *Nature* **439** 419

[201] Shen Y T, Kim T H, Gangopadhyay A K, and Kelton K F 2009 *Phys. Rev. Lett.* **102** 057801

[202] Hodge I M 1995 *Science* **267** 1945

[203] Kirkpatrick T R and Wolynes P G 1987 *Phys. Rev.* A **35** 3072

[204] Gotze W and Sjogren L 1992 *Rep. Prog. Phys.* **55** 241

[205] Hunter G L and Weeks E R 2012 *Rep. Prog. Phys.* **75** 066501

[206] Berthier L and Witten T A 2009 *Europhy. Lett.* **86** 10001

[207] Henderson S I, Mortensen T C, Underwood S M and van Megen W 1996 *Physica* A **233** 102

[208] Zaccarelli E, Valeriani C, Sanz E, Poon W C K, Cates M E and Pusey P N 2009 *Phys. Rev. Lett.* **103** 135704

[209] Huang P Y, Kurasch S, Alden J S, Shekhawat A, Alemi A A, McEuen P L, Sethna J P, Kaiser U and Muller D A 2013 *Science* **342** 224

[210] Mattsson J, Wyss H M, Fernandez-Nieves A, Miyazaki K, Hu Z, Reichman D R and Weitz D A 2009 *Nature* **462** 83

[211] Angell C A 1995 *Science* **267** 1924

[212] Yan L, Düring G and Wyart M 2013 *Proc. Natl Acad. Sci.* **110** 6307

[213] Sessoms D A, Bischofberger I, Cipelletti L and Trappe V 2009 *Phil. Trans. R. Soc.* A **367** 5013

[214] Weeks E R, Crocker J C and Weitz D A 2007 *J. Phys.: Condens. Matter* **19** 205131

[215] Duri A, Sessoms D A, Trappe V and Cipelletti L 2009 *Phys. Rev. Lett.* **102** 085702
[216] Courtland R E and Weeks E R 2003 *J. Phys.: Condens. Matter* **15** S359
[217] Cianci G C and Weeks E R 2007 *Reports of the Institute of Fluid Science* vol 19 (Sendai: Tohoku University) pp 51–6
[218] Cianci G C, Courtland R E and Weeks E R 2006 *Solid State Commun.* **139** 599
[219] Yunker P, Zhang Z, Aptowicz K B and Yodh A G 2009 *Phys. Rev. Lett.* **103** 115701
[220] Di X, Win K Z, McKenna G B, Narita T, Lequeux F, Pullela S R R and Cheng Z 2011 *Phys. Rev. Lett.* **106** 095701
[221] Colin R, Alsayed A M, Castaing J-C, Goyal R, Hough L and Abou B 2011 *Soft Mat.* **7** 4504
[222] Kob W, Donati C, Plimpton S J, Poole P H and Glotzer S C 1997 *Phys. Rev. Lett.* **79** 2827
[223] Adam G and Gibbs J H 1965 *J. Chem. Phys.* **43** 139
[224] Berthier L, Biroli G, Bouchaud J P, Cipelletti L, Masri E D, D L'Hote, Ladieu F and Pierno M 2005 *Science* **310** 1797
[225] Widmer-Cooper A and Harrowell P 2006 *J. Non-Cryst. Solids* **352** 5098
[226] Widmer-Cooper A and Harrowell P 2006 *Phys. Rev. Lett.* **96** 185701
[227] Widmer-Cooper A, Perry H, Harrowell P and Reichman D R 2008 *Nature Phys.* **4** 711
[228] Donati C, Glotzer S C, Poole P H, Kob W and Plimpton S J 1999 *Phys. Rev.* E **60** 3107
[229] Perera D N and Harrowell P 1999 *J. Chem. Phys.* **111** 5441
[230] Parsaeian A and Castillo H E 2008 *Phys. Rev.* E **78** 060105
[231] Hodge I M 1987 *Macromolecules* **20** 2897
[232] Kovacs A J 1964 *Fortschritte Der Hochpolymeren-Forschung* (*Advances in Polymer Science* vol 3/3) (Berlin: Springer) pp 394–507
[233] Higler R, Appel J and Sprakel J 2013 *Soft Matter* **9** 5372–9
[234] Yunker P, Zhang Z and Yodh A G 2010 *Phys. Rev. Lett.* **104** 015701
[235] van Blaaderen A and Wiltzius P 1995 *Science* **270** 1177
[236] Tarjus G, Kivelson S A, Nussinov Z and Viot P 2005 *J. Phys.: Condens. Matter* **17** R1143
[237] Sadr-Lahijany M R, Ray P and Stanley H E 1999 *Physica* A **270** 295
[238] Pronk S and Frenkel D 2004 *Phys. Rev.* E **69** 066123
[239] Hamanaka T and Onuki A 2007 *Phys. Rev.* E **75** 041503
[240] Fecht H 1992 *Nature* **356** 133
[241] Nelson D 1983 *Phys. Rev.* B **27** 2902
[242] Kawasaki T, Araki T and Tanaka H 2007 *Phys. Rev. Lett.* **99** 215701
[243] Royall C P, Williams S R, Ohtsuka T and Tanaka H 2008 *Nature Mater.* **7** 556
[244] Candelier R, Dauchot O and Biroli G 2009 *Phys. Rev. Lett.* **102** 088001
[245] Romeo G, Fernandez-Nieves A, Wyss H M, Acierno D and Weitz D A 2010 *Adv. Mater.* **22** 3441
[246] Hutchinson J 1995 *Prog. Polym. Sci.* **20** 703
[247] Caswell T A, Zhang Z, Gardel M L and Nagel S R 2013 *Phys. Rev.* E **87** 012303
[248] Schreck C F, Bertrand T, O'Hern C S and Shattuck M D 2011 *Phys. Rev. Lett.* **107** 078301
[249] Kegel W K and van Blaaderen A 2000 *Science* **287** 290
[250] O'Hern C S, Langer S A, Liu A J and Nagel S R 2002 *Phys. Rev. Lett.* **88** 075507
[251] Hatano T 2008 *J. Phys. Soc. Japan* **77** 123002
[252] Kaya D, Green N L, Maloney C E and Islam M F 2010 *Science* **329** 656
[253] Henkes S, Brito C and Dauchot O 2012 *Soft Matter* **8** 6092
[254] Chen K, Still T, Schoenholz S, Aptowicz K B, Schindler M, Maggs A C, Liu A J and Yodh A G 2013 *Phys. Rev.* E **88** 022315
[255] Schindler M and Maggs A 2012 *Soft Matter* **8** 3864
[256] Lemarchand C A, Maggs A and Schindler M 2012 *Europhys. Lett.* **97** 48007
[257] Ghosh A, Chikkadi V K, Schall P, Kurchan J and Bonn D 2010 *Phys. Rev. Lett.* **104** 248305
[258] Yunker P J, Chen K, Zhang Z, Ellenbroek W G, Liu A J and Yodh A G 2011 *Phys. Rev.* E **83** 011403
[259] Hasan A and Maloney C E 2012 Inferring elastic properties of an fcc crystal from displacement correlations: sub-space projection and statistical artifacts (arXiv:1212.4868)
[260] Burda Z, Görlich A, Jarosz A and Jurkiewicz J 2004 *Physica* A **343** 295
[261] Mao X, Xu N and Lubensky T 2010 *Phys. Rev. Lett.* **104** 085504
[262] Manning M L and Liu A J 2011 *Phys. Rev. Lett.* **107** 108302
[263] Xu N, Vitelli V, Liu A J and Nagel S R 2010 *Europhys. Lett.* **90** 56001
[264] Chen K, Manning M L, Yunker P J, Ellenbroek W G, Zhang Z, Liu A J and Yodh A G 2011 *Phys. Rev. Lett.* **107** 108301
[265] Ashcroft N W and Mermin N D 1976 *Solid State Phys.* **615**
[266] Gratale M D, Yunker P J, Chen K, Still T, Aptowicz K B and Yodh A G 2013 *Phys. Rev.* E **87** 052301
[267] Fernandes G E, Beltran-Villegas D J and Bevan M A 2008 *Langmuir* **24** 10776
[268] Yodh A G, Lin K, Crocker J C, Dinsmore A D, Verma R and Kaplan P D 2001 *Phil. Trans. R. Soc. Lond.* A **359** 921
[269] Lu P J, Zaccarelli E, Ciulla F, Schofield A B, Sciortino F and Weitz D A 2008 *Nature* **453** 499
[270] Savage J R, Blair D W, Levine A J, Guyer R A and Dinsmore A D 2006 *Science* **314** 795
[271] Zhao C, Yuan G, Jia D and Han C C 2012 *Soft Matter* **8** 7036
[272] Fuchs M and Schweizer K S 2002 *J. Phys.: Condens. Matter* **14** R239
[273] Dijkstra M, van Roij R and Evans R 1999 *Phys. Rev.* E **59** 5744
[274] Likos C N 2001 *Phys. Rep.* **348** 267
[275] Kleshchanok D, Tuinier R and Lang P R 2008 *J. Phys.: Condens. Matter* **20** 073101
[276] Mao Y, Cates M E and Lekkerkerker H N W 1995 *Physica* A **222** 10
[277] Mao Y, Bladon P, Lekkerkerker H N W and Cates M E 1997 *Mol. Phys.* **92** 151–9
[278] Poon W C K, Pirie A D, Haw M D and Pusey P N 1997 *Physica* A **235** 110
[279] Poon W C K and Warren P B 1994 *Europhys. Lett.* **28** 513
[280] Gast A P, Hall C K and Russel W B 1983 *J. Colloid Interface Sci.* **96** 251
[281] Götzelmann B, Evans R and Dietrich S 1998 *Phys. Rev.* E **57** 6785
[282] Joanny J F, Leibler L and De Gennes P G 1979 *J. Polym. Sci. Polym. Phys. Edn* **17** 1073
[283] Asakura S and Oosawa F 1954 *J. Chem. Phys.* **22** 1255
[284] Asakura S and Oosawa F 1958 *J. Polym. Sci.* **33** 183
[285] Vrij A 1976 *Pure Appl. Chem.* **48** 471
[286] Rossi L, Sacanna S, Irvine W T M, Chaikin P M, Pine D J and Philipse A P 2011 *Soft Matter* **7** 4139
[287] Sacanna S, Irvine W T M, Chaikin P M and Pine D J 2010 *Nature* **464** 575
[288] Kaplan P D, Rouke J L, Yodh A G and Pine D J 1994 *Phys. Rev. Lett.* **72** 582
[289] Xing X, Li Z and Ngai T 2009 *Macromolecules* **42** 7271
[290] Fernandes G E, Beltran Villegas D J and Bevan M A 2009 *J. Chem. Phys.* **131** 134705
[291] Meng G, Arkus N, Brenner M P and Manoharan V N 2010 *Science* **327** 560
[292] Sacanna S, Irvine W T M, Rossi L and Pine D J 2011 *Soft Matter* **7** 1631

[293] Bayliss K, van Duijneveldt J S, Faers M A and Vermeer A W P 2011 *Soft Matter* **7** 10345
[294] Debord J D and Lyon L A 2000 *J. Phys. Chem.* B **104** 6327
[295] Debord J D, Eustis S, Byul Debord S, Lofye M T and Lyon L A 2002 *Adv. Mater.* **14** 658
[296] Gao J and Hu Z 2002 *Langmuir* **18** 1360
[297] Hu L, Sarker A K, Islam M R, Li X, Lu Z and Serpe M J 2013 *J. Polym. Sci.* **51** 3004
[298] Reese C E, Mikhonin A V, Kamenjicki M, Tikhonov A and Asher S A 2004 *J. Am. Chem. Soc.* **126** 1493
[299] Mohanty P S, Yethiraj A and Schurtenberger P 2012 *Soft Matter* **8** 10819
[300] Sierra-Martin B and Fernandez-Nieves A 2012 *Soft Matter* **8** 4141
[301] Iyer A S and Lyon L A 2009 *Angew. Chem. Int. Edn* **48** 4562
[302] Muluneh M, Sprakel J, Wyss H M, Mattsson J and Weitz D A 2011 *J. Phys.: Condens. Matter* **23** 505101
[303] Snowden M and Vincent B 1992 *J. Chem. Soc. Chem. Commun.* **16** 1103–5
[304] Hu Z and Xia X 2004 *Adv. Mater.* **16** 305
[305] Gan T, Zhang Y and Guan Y 2009 *Biomacromolecules* **10** 1410
[306] Gan T, Guan Y and Zhang Y 2010 *J. Mater. Chem.* **20** 5937
[307] Cheng D, Wu Y, Guan Y and Zhang Y 2012 *Polymer* **53** 5124
[308] Benee L, Snowden M and Chowdhry B 2002 *Langmuir* **18** 6025
[309] Fraylich M R, Liu R, Richardson S M, Baird P, Hoyland J, Freemont A J, Alexander C, Shakesheff K, Cellesi F and Saunders B R 2010 *J. Colloid Interface Sci.* **344** 61
[310] Cho E C, Kim J-W, Fernandez-Nieves A and Weitz D A 2008 *Nano Lett.* **8** 168
[311] Cho E C, Kim J-W, Hyun D C, Jeong U and Weitz D A 2010 *Langmuir* **26** 3854
[312] Liao W, Zhang Y, Guan Y and Zhu X X 2011 *Macromol. Chem. Phys.* **212** 2052
[313] Liao W, Zhang Y, Guan Y and Zhu X X 2012 *Langmuir* **28** 10873
[314] Lapeyre V, Wolfs M, Sellier E, Leal-Calderon F, Ravaine V and Schmitt V 2011 *Soft Matter* **7** 7689
[315] Monteux C, Marlière C, Paris P, Pantoustier N, Sanson N and Perrin P 2010 *Langmuir* **26** 13839
[316] Trappe V 2013 private communication
[317] Still T, Goodrich C P, Chen K, Yunker P J, Schoenholz S, Liu A J and Yodh A G 2014 *Phys. Rev.* E **89** 012301
[318] Destribats M, Eyharts M, Lapeyre V, Sellier E, Varga I, Ravaine V and Schmitt V 2014 *Langmuir* **30** 1768
[319] Di X, Peng X and McKenna G B 2014 *J. Chem. Phys.* **140** 054903
[320] Wang H, Wu X, Zhu Z, Liu C S and Zhang Z 2014 *J. Chem. Phys.* **140** 024908
[321] Liu Y, Guan Y and Zhang Y 2014 *Macromol. Rapid Commun.* doi:10.1002/marc.201300893
[322] Paloli D, Mohanty Priti S, Crassous J J, Zaccarellic E and Schurtenberger P 2013 *Soft Matter* **9** 3000
[323] Purnomo E H, van den Ende D, Vanapalli S A and Mugele F 2008 *Phys. Rev. Lett.* **101** 238301
[324] Wei G, Zhao C, Hollingsworth J, Zhou Z, Jin F, Zhang Z, Cheng H and Han C C 2013 *Soft Matter* **9** 9924
[325] Joshi R G, Tata B V R and Brijitta J 2013 *J. Chem. Phys.* **139** 124901
[326] Pusey P N 1987 *J. Physique* **48** 709–12
[327] Zaccarelli E, Valeriani C, Sanz E, Poon W C K, Cates M E and Pusey P N 2009 *Phys. Rev. Lett.* **103** 135704
[328] Kosterlitz J M and Thouless D J 1973 *J. Phys. C: Solid State Phys.* **6** 1181
[329] Nelson D R and Halperin B I 1979 *Phys. Rev.* B **19** 2457
[330] Young A P 1979 *Phys. Rev.* B **19** 1855
[331] Nelson D 2002 *Defects and Geometry in Condensed Matter Physics* (Cambridge: Cambridge University Press)
[332] Van Hove L 1950 *Physica* **16** 137
[333] Lohr M A, Alsayed A M, Chen B G, Zhang Z, Kamien R D and Yodh A G 2010 *Phys. Rev.* E **81** 040401